Article

Generation of High Temporal Resolution Fractional Forest Cover Data and Its Application in Accurate Time Detection of Forest Loss

Wenxi Shi [1,2], Xiang Zhao [1,2,*], Hua Yang [1,2], Longping Si [1,2], Qian Wang [1,2], Siqing Zhao [1,2] and Yinkun Guo [1,2]

1   State Key Laboratory of Remote Sensing Science, Faculty of Geographical Science, Beijing Normal University, Beijing 100875, China; wenxi_shi@mail.bnu.edu.cn (W.S.); yh_crs@bnu.edu.cn (H.Y.); silongp@bnu.edu.cn (L.S.); qianwang@bnu.edu.cn (Q.W.); zhaosiqing@mail.bnu.edu.cn (S.Z.); guoyinkun_bnu@mail.bnu.edu.cn (Y.G.)
2   Beijing Engineering Research Center for Global Land Remote Sensing Products, Faculty of Geographical Science, Beijing Normal University, Beijing 100875, China
*   Correspondence: zhaoxiang@bnu.edu.cn; Tel.: +86-010-5880-0181

Abstract: Fractional Forest cover holds significance in characterizing the ecological condition of forests and serves as a crucial input parameter for climate and hydrological models. This research introduces a novel approach for generating a 250 m fractional forest cover product with an 8-day temporal resolution based on the updated GLASS FVC product and the annualized MODIS VCF product, thereby facilitating the development of a high-quality, long-time-series forest cover product on a global scale. Validation of the proposed product, employing high spatial resolution GFCC data, demonstrates its high accuracy across various continents and forest cover scenarios globally. It yields an average fit coefficient of determination (R^2) of 0.9085 and an average root-mean-square error of 7.22%. Furthermore, to assess the availability and credibility of forest cover data with high temporal resolution, this study integrates the CCDC algorithm to map forest disturbances and quantify the yearly and even monthly disturbed trace area within two sub-study areas of the Amazon region. The achieved sample validation accuracy is over 86%, which substantiates the reliability of the data. This investigation offers a fresh perspective on monitoring forest changes and observing forest disturbances by amalgamating data from diverse sources, enabling the mapping of dynamic forest cover over an extensive time series with high temporal resolution, thereby mitigating data gaps and enhancing the precision of existing products.

Keywords: fractional forest cover; GLASS FVC; forest loss; CCDC

1. Introduction

Forests, as the largest carbon reservoir in terrestrial ecosystems, significantly impact the carbon sequestration function of land-based systems. Their vital role includes maintaining ecological balance, facilitating carbon cycling, mitigating climate change, and determining energy budgets [1–3]. In contrast, the global occurrence, severity, and scope of forest disturbances have witnessed a notable escalation in the 21st century, primarily attributed to climate change-induced factors such as droughts, wildfires, and pest outbreaks. Additionally, anthropogenic logging activities have also contributed to this phenomenon [4,5]. Hence, it is imperative to obtain precise and timely forest cover data, which can furnish robust evidence to elucidate the spatial and temporal fragmentation patterns of forests, as well as their underlying causes. Moreover, such information is essential for comprehending the ramifications of forest disturbances on climate change, biodiversity, and other related facets. The Fractional Forest Cover (FFC) refers to the ratio of the area of forest canopy viewed from the vertical direction to the entire pixel [6–8]. In 2015, the United Nations General Assembly established 17 sustainable development goals (SDGs), one of which

specifically highlights FFC as an important parameter for protecting, restoring, and promoting sustainable management of forest resources [9]. A prolonged temporal sequence of fractional forest cover data holds the potential to offer precise and reliable information on forest attributes, thereby enhancing the efficacy of natural resource management.

Remote sensing data has traditionally served as the principal data source for mapping Fractional Forest cover (FFC), particularly in the context of large-scale and long-term regional studies. Over the past years, a limited number of Fractional Forest cover (FFC) maps spanning a global scale have been developed, indicative of the increasing significance attributed to this research domain. Notable examples include the Terra MODIS Vegetation Continuous Fields (MODIS VCF) [10,11], the Global Forest Cover Change (GFCC) Tree Cover [12], the forest cover map by the Japan Aerospace Exploration Agency (JAXA) [13], and the Hansen Global Forest Change dataset (The Hansen GFC) [14,15]. Notably, the latter provides FFC data at a resolution of 30 m for the years 2000 and 2010, along with comprehensive annual information on global forest loss and gain. At the same time, Landsat and other high spatial resolution remote sensing data have increasingly been applied to generate global Fractional Forest cover (FFC) datasets [7,8,16]. However, it is essential to note that medium spatial resolution FFC remains crucial for understanding the dynamics and long-term trends of forest ecosystems. For one thing, the spatiotemporal scale remains crucial for a comprehensive understanding of global forest greening under gradual and abrupt climate changes [17]. For another, using long time series remote sensing data with a spatial resolution of 30 m or even higher for large-area change detection results in a substantial increase in data volume, requiring more time and effort for processing and computation [18–20]. Tang et al. have suggested the utilization of medium spatial resolution data for large-scale near real-time operational monitoring of forest loss, followed by the strengthening of monitoring in target areas (such as deforestation "hotspots") using high-resolution data [21,22]. Consequently, there is a growing interest in investigating fractional forest cover information and the associated forest change dynamics at moderate resolutions.

Currently, there is a lack of comprehensive datasets enabling the observation of dynamic changes in global FFC on both an intra-annual and inter-annual basis [23–25]. The update frequency of MODIS VCF is limited to an annual cycle, while that of GFCC is constrained to a five-year interval. The complexity of defining FFC data, necessitating differentiation between forest types, non-forest vegetation types, and non-vegetated areas, precludes the feasibility of simulating this parameter using a binary pixel model. Moreover, the distinction between forest and non-forest vegetation types requires extensive sample data for model training due to spectral and structural similarities, rendering it challenging to achieve updates at monthly or higher frequencies [16,26,27]. Other multi-temporal vegetation indices and land classification products are subject to limitations [28,29]. While indices like the Normalized Difference Vegetation Index (NDVI), Enhanced Vegetation Index (EVI), and Leaf Area Index (LAI) aim to capture the greenness of forest vegetation, they fail to unequivocally attribute these changes to specific sources such as forest trees, understory grasses, or shrubs [30]. The utilization of hard land-use classification products results in the provision of multi-period forest distribution maps. Nonetheless, these datasets impose specific canopy cover thresholds to delineate forests, potentially causing an overestimation of forest coverage in areas with low tree density [25,31]. The 8-day updated Global Land Surface Satellite Fractional Vegetation Cover (GLASS FVC) stands as one of the most mature and commonly utilized global land surface characteristic parameter datasets [32,33]. Hence, a pertinent topic for consideration and exploration lies in the extraction of forest-related information from established vegetation cover datasets and the subsequent construction of a novel time series for FFC. Acquiring a higher frequency time series of FFC is of paramount significance for comprehensive, timely, and accurate observation of forest disturbances and dynamic deforestation monitoring.

Therefore, this study endeavored to create a fractional forest cover product named Global Land Surface Satellite Fractional Forest Cover (GLASS FFC), of which the spatial resolution is 250 m and is at an 8-day interval. Through a synergistic utilization of the

GLASS FVC product and MODIS VCF, we aimed to not only mitigate data shortcomings but also elevate the precision of existing products. To ensure the reliability and accuracy of the GLASS FFC product, a comprehensive global-scale accuracy assessment will be conducted. This evaluation will provide crucial insights into the performance and limitations of the developed product, enabling its widespread use in forest change monitoring studies in the future. Furthermore, to demonstrate the efficacy of GLASS FFC data in detecting forest changes, we employed GLASS FFC products as the data source and combined them with the CCDC algorithm to achieve rapid mapping of forest loss areas across a large geographical extent. This endeavor serves as a foundational step towards conducting detailed investigations on forest loss at regional and even global scales in the future. This research endeavor will facilitate more targeted conservation and management efforts, contributing to effective decision-making and sustainable forest resource utilization.

2. Materials and Methods

2.1. Data and Workflow

This study developed and applied high-temporal resolution fractional forest cover data. (1) Initially, a global FFC dataset, referred to as GLASS FFC, was created for the period spanning from 2000 to 2020 at a spatial resolution of 250 m, with an 8-day temporal frequency. The primary data source used to construct this dataset was GLASS FVC data, which was further enhanced through the integration of the Global Land Surface Satellite Enhanced Vegetation Index (GLASS EVI) and MODIS VCF. (2) Subsequently, the accuracy of GLASS FFC was assessed by comparing it with high-resolution GFCC data. The Global Ecosystem Dynamics Investigation level2B (GEDI02_B) data obtained from lidar technology and land cover data, the Global 30 m Land-Cover products with Fine Classification System (GLC_FCS30D) were also involved in the supporting validation. (3) Finally, leveraging GLASS FFC as the primary data source and employing the CCDC algorithm, the study investigated and analyzed forest loss occurrences within the study area. The detection results were then compared and validated against the Hansen GFC data. This comprehensive exploration allowed for the assessment of the usability and advantages of the GLASS FFC dataset constructed in this research endeavor. The specific datasets utilized in this study were introduced in the subsequent section.

2.1.1. Vegetation Index Data

GLASS FVC is a key indicator for monitoring the health and productivity of terrestrial ecosystems [33]. The training data was generated using Landsat TM/ETM+ reflectance data, which was transformed into NDVI data. The pixel dichotomy method was then applied to calculate the pixel's mean value at 500 m [34]. To train the FVC model, a Multivariate Adaptive Regression Splines (MARS) algorithm was used [32]. This algorithm is a non-parametric regression method that can effectively capture the complex relationships between input variables and output values. The trained model was then applied to MODIS reflectance data as input to produce global 500 m FVC data. The FVC data is updated every 8 days, providing a near-real-time monitoring capability for global forest cover [35,36].

GLASS EVI is a new global seamless 250 m, 8-day EVI product for 2000–2021 developed from Moderate Resolution Imaging Spectroradiometer (MODIS) surface reflectance data using a Long Short-Term Memory (LSTM) neural network approach [37]. The EVI data minimizes variations in the canopy background and retains its sensitivity even under dense vegetation conditions. Moreover, compared to MODIS EVI, the GLASS EVI data exhibits a more uniform quality. In this study, we utilize the GLASS EVI data as the basis for downscaling GLASS FVC.

2.1.2. Relevant Fractional Forest Cover Data

MODIS VCF is a sub-pixel representation of global surface vegetation estimation [10]. Each pixel provides the percentages of tree cover, non-tree vegetation cover, and bare type instead of simple classification results. The current resolution of MODIS VCF is 250 m, and

it is updated annually. MODIS VCF employs a regression tree algorithm, incorporating linear regression functions to the algorithm's nodes, thus facilitating the detection of data variability while increasing precision and minimizing noise. It generates a comprehensive, annually updated global-scale dataset of FFC utilizing MODIS reflectance data as the primary input source [10]. Validation utilizing laser radar imagery has confirmed that the MODIS VCF has an overall accuracy of more than 70% on a worldwide scale [11,38,39]. In this study, we primarily downloaded and utilized MODIS VCF on Google Earth Engine.

GFCC dataset [12] provides estimates of the horizontal ground percentage covered by woody vegetation with a height greater than 5 m for each 30-m pixel. This dataset is updated globally for the years 2000, 2005, 2010, and 2015. GFCC Tree Cover, initiated by Hansen et al., utilizes an improved Cubist algorithm, drawing from Landsat reflectance data as the data source, thus further enhancing the resolution of MODIS VCF. The validation accuracy of GFCC is confirmed to exceed 85% at four global locations [12]. In this study, we primarily downloaded the GFCC dataset using the Google Earth Engine (GEE) platform. Using the 2015 data as a reference, we conducted a global validation of the GLASS FFC dataset.

GEDI02_B data [40] is derived from the Global Ecosystem Dynamics Investigation (GEDI) lidar sensor, which captures biophysical metrics extracted from each GEDI waveform. The vertical spacing between leaf-level measurements is consistently 5 m. The data is provided in a point-based format with a spatial resolution (average footprint) of 25 m, covering a global range from 51.6°N to 51.6°S. In this study, we primarily downloaded the GEDI02_B data using the Google Earth Engine (GEE) platform. The "canopy cover" is defined in the product as the percentage of the ground covered by the vertical projection of canopy material, including leaves, branches, and stems [41], which aligns closely with the definition of forest canopy cover in optical remote sensing products [42–44]. The data was utilized to validate the GLASS FFC dataset, specifically in the Amazon tropical rainforest region [45].

2.1.3. Land Cover Data

GLC_FCS30D represents the first global 30-m resolution land cover product that incorporates continuous change detection technology [46]. It employs an elaborate classification system featuring 35 land cover categories, including more than ten types specifically related to forests, and spans the period from 1985 to 2022. The update frequency of this product was quinquennial prior to the year 2000 and became annual thereafter. The development of GLC_FCS30D involved the integration of continuous change detection methodologies, local adaptive updating models, and spatiotemporal optimization algorithms using dense time-series Landsat imagery. The overall accuracy of the ten primary land cover types within the baseline classification system is documented at 80.88% ($\pm$0.27%). In this study, we predominantly utilize this data to facilitate the validation of the accuracy of GLASS FFC.

2.1.4. Forest Cover Change Data

The Hansen GFC dataset [14] is the result of a time-series analysis of Landsat satellite imagery, aiming to determine global forest extent and change characteristics. It has been widely utilized in studies analyzing forest loss and gain as well as the driving factors in various countries and regions [47–49]. The accuracy of Hansen GFC has been assessed by comparing and validating it against ground-truth data, such as local forest management inventories and forestry measurement reports, consistently achieving accuracy levels above 90% [50–52]. Therefore, the combination of Hansen GFC data with GEVI (Google Earth-based visual interpretation plots) provides a reliable and efficient approach for validating forest loss detection results. Additionally, the open access and transparency of the Hansen GFC dataset enhance the reproducibility and credibility of the forest loss validation process.

2.2. Long-Term Dynamic Fractional Forest Cover Mapping Based on GLASS FVC and MODIS VCF

2.2.1. Decomposition of GLASS FVC

This study initially implemented a downscaling approach to decompose GLASS FVC into a spatial resolution that is consistent with MODIS VCF data. Drawing from the principles of pixel unmixing models, this method assumes that coarse-resolution FVC pixels are the linear combinations of finer-resolution FVC pixels. All finer-resolution pixels within a coarse-resolution pixel are regarded as endmembers of the coarse-resolution pixel, with weights determined by vegetation growth status. NDVI still has some problems while being applied, e.g., saturation problems found in highly denied vegetation, etc. To account for these issues, the Enhanced Vegetation Index (EVI), a commonly used vegetation index that outperforms NDVI in reducing background and atmospheric effects and saturation issues, was used as the weight for each end member during the decomposition process.

Initially, GLASS FVC was resampled to a spatial resolution of 250 m × 250 m using bilinear interpolation. Subsequently, a 2 × 2 window of 250 m pixels was employed to match and decompose the resampled GLASS FVC data pixel by pixel, with pixel values calculated using Formula (1). To minimize non-vegetation interference, pixels with EVI values below 0.05 were considered non-vegetation and were excluded from the decomposition process.

$$FVC_D = \frac{EVI_D \sum_{i=1}^{M} fvc_i}{\sum_{i=1}^{M} EVI_I} \tag{1}$$

where FVC_D is the decomposed *FVC* value of the pixel and EVI_D is the corresponding *EVI* value. *M* is the number of valid vegetation endmembers within the moving window, and fvc_i and EVI_I represent the resampled *FVC* and *EVI* values, respectively.

2.2.2. Extraction of High Temporal Resolution FFC

This study initially employed a weighting methodology to downscale the GLASS FVC using the 250 m resolution GLASSEVI, resulting in the generation of vegetation coverage data with a spatial resolution of 250 m and an update frequency of 8 days. Due to the considerable uncertainty associated with the MCD12Q2 product and the intricate seasonal patterns, particularly in tropical regions, the decision was made to forego the utilization of the MODIS EVI product. Instead, the unreleased GLASS EVI product was referenced. Subsequently, for a more precise delineation of the FFC using the downscaled data, the 'percent tree cover' and 'percent non-tree vegetation cover' bands were extracted from the MODIS VCF product, which possesses a spatial resolution of 250 m. The proportion of forest types was then calculated based on the vegetation coverage data at the 250 m pixel level. The GLASS FFC was derived through the multiplication of the previously obtained results, followed by post-processing and the application of system bias correction. This comprehensive process yielded 8-day, 250 m resolution global FFC data.

2.3. Mapping of Long-Term Forest Loss Based on CCDC

Consequently, this study endeavors to employ the CCDC algorithm [53,54] to fully leverage the temporal information derived from the GLASS FFC time series, enabling a rapid and comprehensive screening of areas affected by forest disturbances.

The CCDC algorithm is widely used for monitoring and analyzing land cover changes, including forest disturbances [55–57]. It offers a comprehensive approach that combines change detection and classification techniques to identify and characterize temporal changes in satellite imagery. In the CCDC algorithm, the time series data is first decomposed into different components using harmonic analysis. This decomposition separates the time series into its constituent parts, including a constant term representing the overall mean, intra-annual variations capturing seasonal patterns, and inter-annual trends depicting long-term changes. To detect changes, the CCDC algorithm employs a statistical approach based on the comparison between the fitted historical model and the residuals

of the incoming data. The residuals represent the differences between the observed pixel values and the values predicted by the model.

The CCDC version employed in this study, based on Chen et al. [55], utilizes the Root Mean Square Error (RMSE) comparison between the fitted historical model and the residuals of the incoming data for change detection. When the residuals deviate from the model for six consecutive observations, it suggests a significant change has occurred. The date of the first deviation is then identified as the date of change. However, it is important to note that not all detected breaks by the CCDC model necessarily indicate forest disturbances. Other factors such as sensor noise, cloud cover, or changes in land use and land cover types can also contribute to detected breaks. Therefore, further analysis and contextual information are typically required to accurately interpret the detected changes and determine if they are related to forest loss or other factors.

2.4. Performance Validation Methods

2.4.1. Validation of GLASS FFC Product

Assessing and validating continuous estimations at moderate resolutions can often be challenging due to the heterogeneity of the ground, which makes it impractical to directly employ ground measurement values for validation purposes. In our study, we opted to utilize the higher-resolution continuous forest estimation product, GFCC, and upscale its values to moderate spatial resolution pixels (it is worth noting that the tiling and projection of GLASS FFC align with the MODIS series 250-m grid products). Subsequently, we conducted an evaluation and comparison with the results of GLASS FFC. The GFCC dataset was initially reprojected to the MODIS sinusoidal projection at a resolution of 30 m. To match the gridding, we applied the exact area averaging method to generate the final dataset on the MODIS sinusoidal 250-m grid. To quantify the uncertainty, we employed commonly used data validation metrics, namely mean absolute error (MAE), root-mean-squared error (RMSE), and R-squared (R^2), which are based on the linear relationship and average differences between paired data values.

$$MAE = \frac{1}{N}\sum_{i=1}^{N}|y_i - \hat{y}_i| \tag{2}$$

$$RMSE = \sqrt{\frac{1}{N}\sum_{i=1}^{N}(y_i - \hat{y}_i)^2} \tag{3}$$

$$\overline{y}_i = \frac{1}{N}\sum_{i=1}^{N}y_i \tag{4}$$

$$R^2 = 1 - \frac{\sum_{i=1}^{N}(y_i - \hat{y}_i)^2}{\sum_{i=1}^{N}(y_i - \overline{y}_i)^2} \tag{5}$$

In the context, N represents the sample size, where y_i denotes the reference value (GFCC) of the i-th sample, $\hat{y}$ represents the predicted value (GLASS FFC) of the ith sample.

In consideration of the inherent errors associated with the GFCC product, an extensive spatial comparison of the GLASS FFC was initiated using the 30-m land cover product from 2015, denoted as GLC_FCS30D. Given the refined classification of forest types in GLC_FCS30d, which encompasses more than ten categories, and mindful of the efficiency and complexity of data validation, selected regional subsets of different forest types were employed. By examining the spatial distributions and frequency statistics of GLC_FCS30D, GFCC, and GLASS FFC, the spatial accuracy of GLASS FFC was assessed. The forest types from GLC_FCS30D were aggregated based on secondary classification definitions to a resolution of 250 m, and the continuous forest coverage for each pixel was computed. The frequency histograms of GLC_FCS30D, GFCC, and GLASS FFC across the various forest-type study areas were analyzed to observe peak occurrences and overlaps as indicators of spatial consistency among the datasets.

2.4.2. Validation of the Forest Loss Identification

To validate the derived findings pertaining to forest loss, we conducted a comprehensive collection of numerous sample plots from three distinct sources, encompassing PRODES (the Amazon Deforestation Monitoring Project) and GEVI (Google Earth visual interpretation). PRODES, which is managed by the Brazilian Space Agency, Instituto Nacional de Pesquisas Espaciais (INPE) [58], facilitated the acquisition of digital spatial data layers pertaining to deforestation. These data layers were derived from INPE's extensive PRODES dataset, which spans over a long-term period. The purpose of obtaining these data layers was to overlay them with degradation layers in order to analyze the changes that occurred in OYs from 2000 to 2018 [58]. We randomly selected sample plots from the PRODES dataset to validate the results of forest loss in the Amazon region. Visual interpretation constituted the predominant method employed for validation in this investigation to augment the sample size and enhance its representativeness. The process of sample selection on Google Earth entailed a comparative analysis of high-resolution imagery from various time intervals, facilitating the identification of central regions associated with extensive deforestation or fire occurrences. By synergistically leveraging extensive classification expertise, the sample points indicative of forest loss were promptly and accurately ascertained from the Google images.

The evaluation of forest loss detection, gain area estimation, and spatial distribution entailed the utilization of multiple metrics, including user accuracy, producer accuracy, overall accuracy, and the Kappa Coefficient. User accuracy primarily focuses on assessing the model's sensitivity and recognition capability, specifically its ability to accurately identify true positive instances. Conversely, producer accuracy emphasizes the model's precision and accuracy in predicting positive cases. Overall accuracy represents the arithmetic mean of user accuracy and producer accuracy, with a higher value indicating greater robustness of the outcomes. Another vital accuracy metric employed is the Kappa Coefficient, which measures the degree of concordance between the classified results and random allocation values. A Kappa Coefficient approaching 1 signifies a heightened resemblance between the classified image and the corresponding ground truth. Furthermore, we conducted a comparative analysis between the annually identified forest loss results and the Hansen Global Forest Change (Hansen GFC) data to assess spatial consistency. Additionally, the dissimilarities between the two datasets were quantified through the calculation of annual loss areas.

3. Results

3.1. Spatial Patterns and Time Series of GLASS FFC

Figure 1 illustrates the distribution of the mean spatial values of fractional forest cover data from the GLASS FFC constructed for the year 2020. To assess the intra-annual spatial variations of GLASS FFC across the globe, the four panels in Figure 1 represent composite mean values for the months of January, April, July, and October, each indicative of a different season. The results reveal that regions such as the Amazon, the Congo Basin, and the subtropical rainforests of Southeast Asia are characterized by concentrations of forest coverage exceeding 90%, with minimal variation throughout the different months. In contrast, the southern forests of North America and Eurasia, along with the dense temperate forests of the Northern Hemisphere, exhibit forest coverage rates above 90% in July but drop to between 30 and 70% in other seasons. Forests outside the tropical rainforest zones in South America and Africa consistently display forest cover ranging from 40–90% across all seasons. In agricultural, grassland, and desert areas, the estimated forest coverage throughout all four seasons approximates 0%, accounting for about 55% of the global land area.

To emphasize the temporal characteristics of the GLASS FFC, we approached the analysis from two distinct perspectives: land cover differences and forest cover changes. From these perspectives, time series curves based on individual pixels were constructed, providing a detailed depiction of temporal dynamics within the dataset.
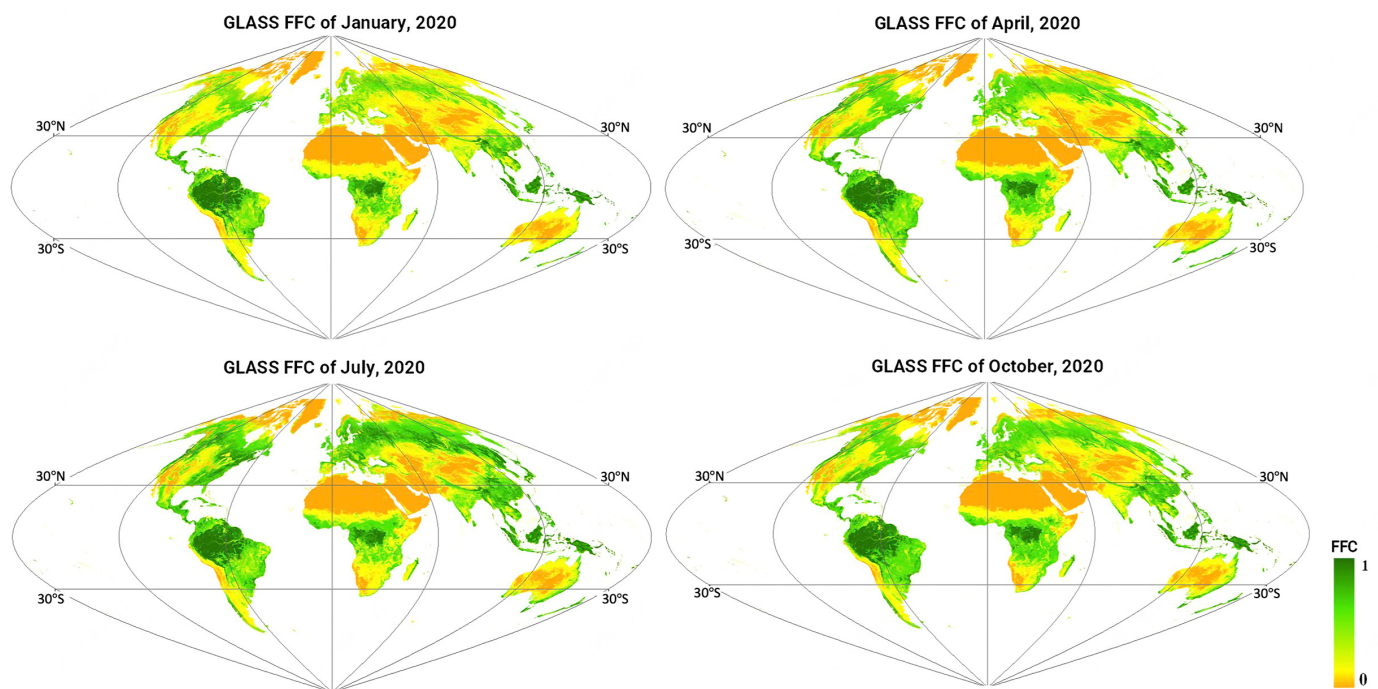
Figure 1. Global maps of the GLASS FFC products corresponding to different days in the four seasons of 2020. The Antarctic Territories are not included in the map.

For the first component, we selected a study region situated within the subtropical monsoon zone of Southeastern Asia, known for its distinct seasonal patterns. Within this area, we generated time series curves based on pixels representing diverse land cover types. These curves depicted the temporal trajectories of GLASS FVC, GLASS FFC, and the concurrent non-tree vegetation percent. To mitigate the potential impact of spatial misalignment, we resampled the GLASS FFC data to a 500-m spatial resolution, aligning it with the grid of the GLASS FVC product. As illustrated in Figure 2a–f, the six sets of time series curves exhibit distinct seasonal trends, with the trajectories of FVC and FFC displaying a generally consistent pattern of variation. However, due to the prior downscaling algorithm employed for GLASS FVC and the forest information provided by the MODIS VCF product, there are minor differences in the finer details of the respective curves.

Furthermore, the high-resolution temporal curves of FVC and FFC data provide a novel perspective for differentiating various land cover types. For instance, Figure 2b,c represent forested areas, where both FVC and FFC exhibit relatively high values. In contrast, Figure 2a,e depict cropland and grassland, respectively, which are non-forest vegetation types, and their FVC and non-tree vegetation percent time series curves align closely. Figure 2d represents a shrubland type, where the FVC peak exceeds 0.5, while the FFC and non-tree vegetation percent are both relatively low and converge. Lastly, Figure 2f illustrates a wetland type characterized by FVC values below 0.5, FFC values below 0.1, and a relatively muted seasonal trend.

In the second part, to further validate the effectiveness of the GLASS FFC dataset in capturing forest cover changes, we plotted the time curves of pixels exhibiting forest status between 2000 and 2020 (Figure 3). Specifically, we selected pixels from two tropical regions (Figure 3a,b) and two subtropical regions that exhibit seasonal variations (Figure 3c,d). The proposed method effectively captures the dynamic changes in FFC over time, including distinct seasonal patterns and growth characteristics. Additionally, the time curves provide insights into instances of forest loss observed in four distinct pixel areas during specific time periods. We verified the detection of these changes using high-resolution historical remote sensing imagery from Google Earth, which confirmed the continuity and accuracy of the

time curves of the GLASS FFC product. These findings serve as a testament to the potential of GLASS FFC in effectively monitoring the dynamic shifts in global forest coverage.
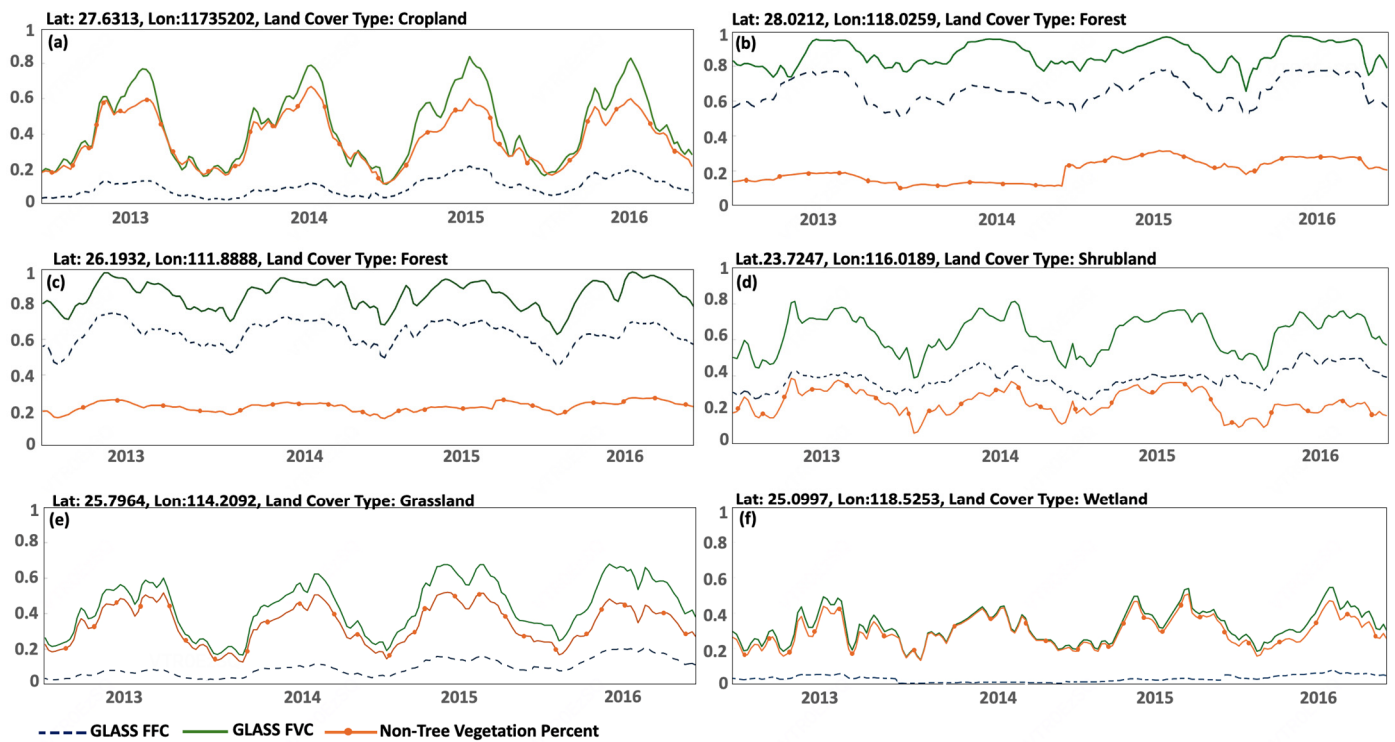
Figure 2. Comparative Analysis of Pixel-based GLASS FVC, GLASS FFC, and Corresponding Non-Tree Vegetation Percent Time Series across Different Land Cover Types. (**a**) Cropland; (**b**,**c**) Forest; (**d**) Shrubland; (**e**) Grassland; (**f**) Wetland.
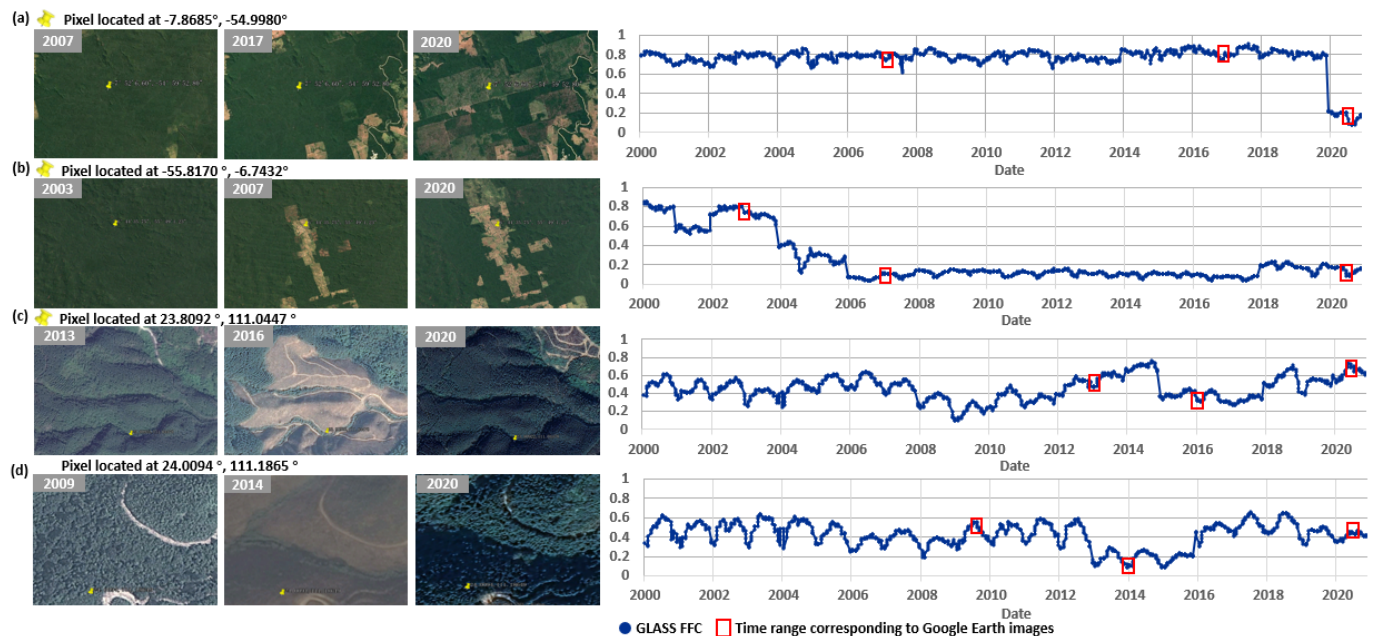

Figure 3. Time series plot of GLASS FFC on a single 250 m image element and examples of Google Earth image temporal changes in the corresponding area. The locations described in panel (**a**) and panel (**b**) are situated in the tropical rainforest region, while panels (**c**,**d**) are in the subtropical evergreen broadleaved forest.

3.2. Accuracy Evaluation and Product Comparison of GLASS FFC

To validate the GLASS FFC product, we conducted a multi-scale assessment, examining its performance at both the global and local levels. At the global scale, we compiled a dataset of 113 validation sites based on the guidelines established by the CEOS-LPV initiative (Garrigues et al., 2008) [59]. These validation sites were selected to be homogeneous in terms of land cover type, vegetation composition, and topography, with minimal proportions of urban areas and permanent water bodies, making them suitable for vegetation index validation. For each site, we extracted the GLASS FFC and the GFCC data, which had been resampled to a 250-m resolution within a 3 km by 3 km area centered on the site location, to assess the product accuracy. Figure 4b depicts the global distribution of the 113 validation sites, from which a total of 202,356 validation pixels were extracted.
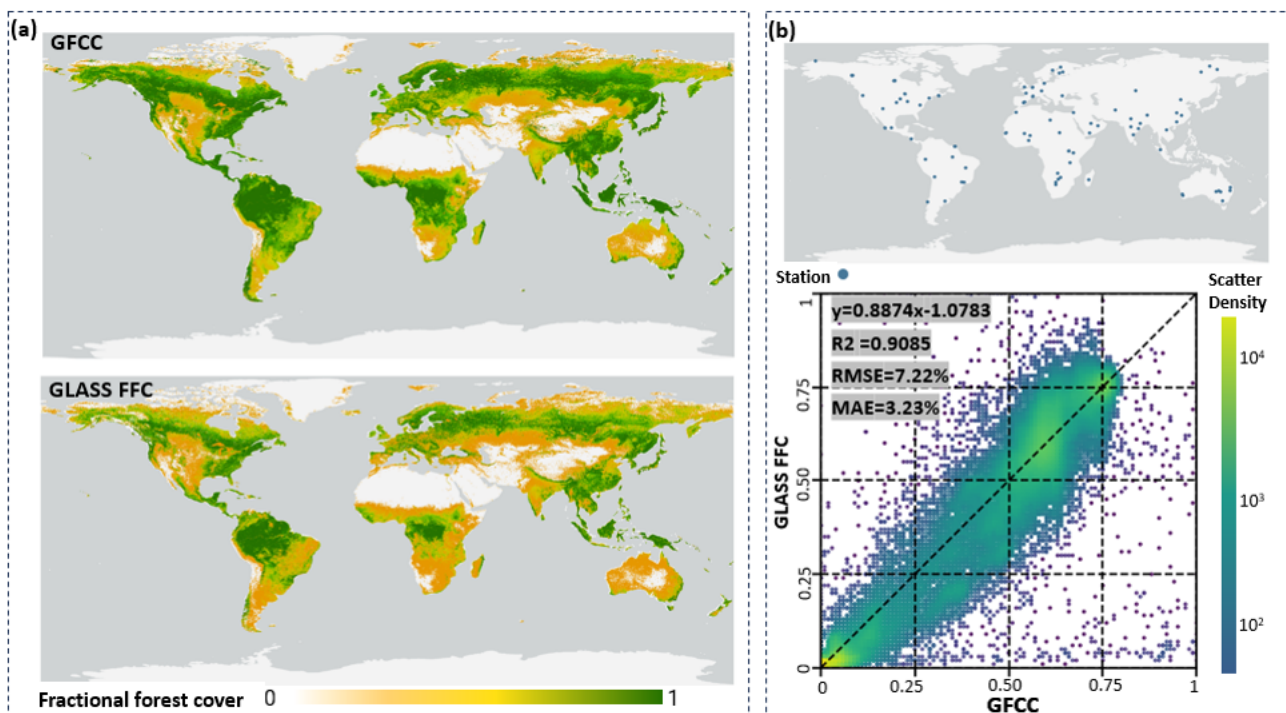
Figure 4. Comparison of fractional forest cover between GLASS FCC and GFCC. (**a**) Global Spatial Distribution of GLASS FFC and GFCC in 2015. (**b**) Global Spatial Distribution of Sites and Site-based Data Scatter Plot with Validation Accuracy.

Additionally, we selected four distinct geographic regions representing different continents and climate zones, exhibiting diverse forest landscapes, as our primary study areas. This allowed us to determine the local-scale accuracy of the GLASS FFC product across different climatic regimes and spatial extents. These four study regions encompass territories in Asia, specifically the northwestern Shaanxi Province in China; Africa, specifically the central rainforest border of the Republic of Congo; South America, specifically the central Rondônia State in Brazil; and North America, particularly the eastern part of British Columbia in Canada. Figure 5a presents the spatial locations of four study sample areas, using GLASS FFC as the map background. The red dots represent the location of the selected sample region.
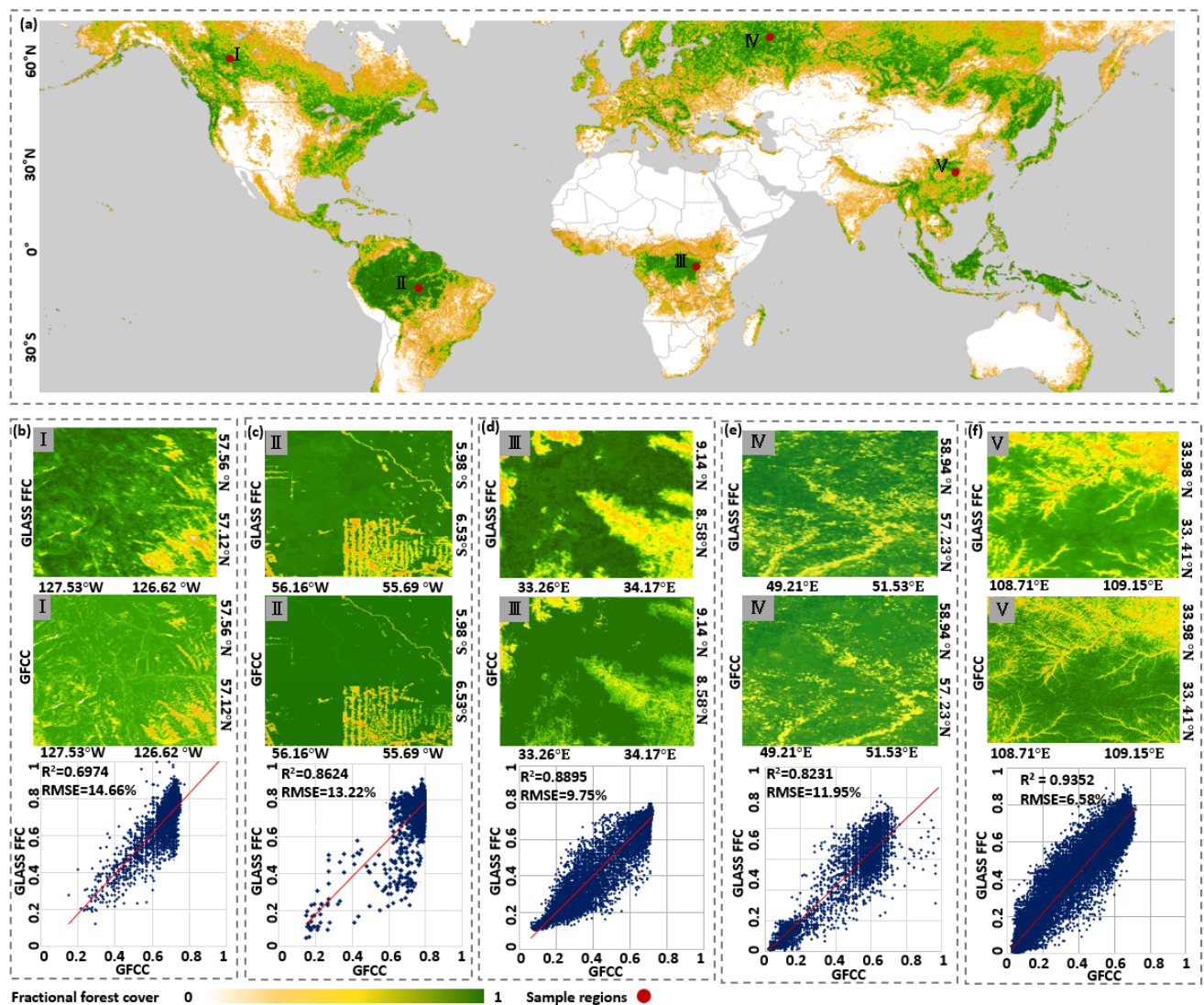
Figure 5. Comparison of GLASS FFC with GFCC in different validation regions in different continents and climate zones. The red line in the scatter plot is the linear regression line that fits the paired data points in 2015. (**a**) Global Spatial Distribution of Four Regions (**b**) Study region in North America (GLASS FFC = 0.0365 + 1.0827 × GFCC, R^2 = 0.6879, RMSE = 14.03%). (**c**) Study region in South America (GLASS FFC = −2.7669 + 1.0238 × GFCC, R^2 = 0.8624, RMSE = 13.12%). (**d**) Study region in Africa (GLASS FFC = 0.01 + 0.9981 × GFCC, R^2 = 0.8895, RMSE = 9.75%). (**e**) Study region in Europe (GLASS FFC = 0.051 + 1.0355 × GFCC, R^2 = 0.8231, RMSE = 11.95%). (**f**) Study region in Asia (GLASS FFC = 0.0024 + 1.0897 × GFCC, R^2 = 0.9352, RMSE = 6.58%).

Figure 4a illustrates the results aggregated to a 250-m resolution from the GFCC dataset for the year 2015, alongside the annual average results from the GLASS FFC for the same year, whereas Figure 4b displays the distribution of validation sites and a scatter plot comparing the consistency between the datasets. The synthesized GLASS FFC dataset demonstrates a high degree of consistency with the validation GFCC data, with a coefficient of determination (R^2) exceeding 90%. The MAE and the RMSE are quantified as 3.23% and 7.22%, respectively. Additionally, the fitted regression line approaches a slope of approximately 0.89, reflecting the annual composite nature of the 46 GLASS FFC data images, which tend to slightly underestimate forest coverage in regions with seasonal variations compared to the GFCC. Furthermore, due to the coarser resolution, it has been observed that in predominantly non-forest areas, such as urban zones, the synthesized

dataset underestimates areas with sparse tree canopy distribution, indicating a lower detection sensitivity in regions with minimal forest cover.

Figure 5 illustrates the validation results for the four selected study areas. Figure 5b–f displays these scatter plots, providing a visual representation of the data. In the eastern part of British Columbia Province, Canada, and the central region of Rondônia State, Brazil, the R^2 values were both below 0.87, with an RMSE exceeding 13% (as illustrated in Figure 5b,c). Sexton et al. observed that estimates of forest cover in the Americas, based on GFCC data, tend to be overestimated compared to lidar data from locations such as California and Costa Rica [12]. Consequently, employing GFCC as the validation data in this study results in an overall underestimation of forest coverage in the Americas region. In Europe, we selected the Kologriv virgin forest area located in the northern part of Kostroma Oblast, Russia, as the study area. The value of R^2 was 0.75, and the value of GLASS FFC was slightly higher (Figure 5e). In the northwestern region of Shaanxi Province, China (Figure 5f), a linear regression analysis was conducted to compare the values of GLASS FFC with those of GFCC. The analysis resulted in an R^2 value of 0.935, indicating that, on average, GLASS FFC values were slightly lower. Similarly, in the tropical rainforest region of central Africa, the R^2 value was 0.890, with GLASS FFC values slightly higher, particularly towards the upper end of the range (as illustrated in Figure 5d). This disparity can be attributed to the geographical separation of the three study regions, leading to variations in the timing of peak vegetation. Additionally, GFCC provides data for only one period per year, which introduces systematic differences when compared to the average data of GLASS FFC.

Furthermore, as shown in Figure 6, we conducted an analysis based on the extraction of GLASS FFC from four distinct forest regions, namely mixed temperate forest, mixed cold-temperature forest, tropical rain forest, and tropical seasonal forest. The FFC from these regions were compared with the GFCC and the GLC_FCS30D at a resolution of 250 m. Additionally, we computed the percentage histogram of FFC for each of the four regions. The comparative analysis revealed a consistent estimation of different forest types using our proposed approach. Within the tropical rainforest region, there exists a significant presence of dispersed high-density forest cover. The FFC percentage estimated by our method consistently exceeds 80% and exhibits a reasonable transition toward the peripheral areas. In the region of tropical seasonal forests, the peak of the forest cover percentage is observed at around 20%, representing cultivated land, while another peak is observed at approximately 60%, which corresponds to closed deciduous broadleaved forests. However, in comparison to GFCC and GLC_FCS30D, the peak values exhibit a certain left-skewness. This can be attributed to the fact that GLASS FFC calculates the annual average values. In the mixed temperate forest region, a substantial amount of forest cover below 60% is extracted, with peaks observed at around 5% and 50%. These peaks capture the linear distribution of trees surrounding agricultural fields, and the estimated values range from 10% to 30%. And in the mixed cold-temperature forest region, the peaks are primarily concentrated between 20% and 60%. This range captures the transitional zones from open deciduous broadleaved forests to bare areas. This pattern is similar to the results obtained from GLC_FCS30D. However, GFCC shows a greater concentration of forest cover, around 5%.

To summarize, these results reveal the remarkable accuracy and reliability of the data, instilling confidence in its suitability for a wide range of applications worldwide. However, considering the inherent errors associated with the GFCC product, it is crucial for future research to prioritize the attainment of more precise validation through meticulous field investigation data. This approach will enhance the credibility of the product and establish it as a reliable tool for monitoring changes in forest coverage.
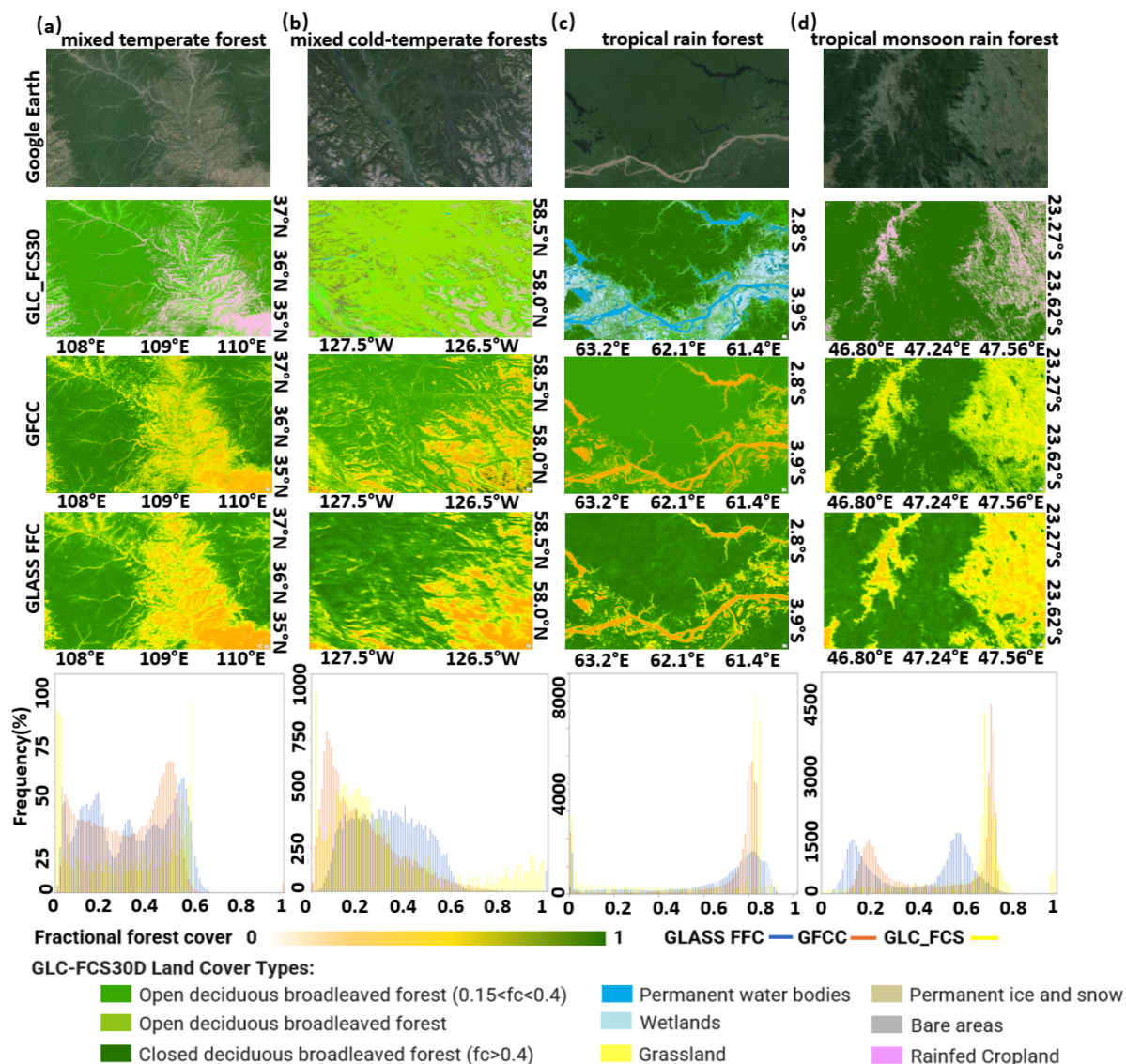
Figure 6. Comparative Spatial Distribution and Frequency Histograms of Three Products across Different Forest Types. (**a**) Mixed temperate forest; (**b**) Mixed cold-temperate forests; (**c**) Tropical rain forest; (**d**) Tropical monsoon seasonal forest.

3.3. Forest Loss Identification Based on GLASS FFC and CCDC

To further investigate the applicability of GLASS FFC in monitoring forest changes and to leverage the advantages of its long-term, high-resolution time series data, we conducted a rapid assessment of forest loss areas in the Amazon region from 2000 to 2020. This analysis was performed using the Google Earth Engine (GEE) platform in conjunction with the CCDC algorithm.

3.3.1. Post-Processing of the CCDC

The CCDC algorithm can detect significant temporal discontinuities in time series data, but it cannot definitively confirm that the detected breakpoints are caused by forest loss. To determine the most appropriate metric for identifying forest disturbance-related breaks, we followed the methodology and parameter selection described by Chen et al. and decided to utilize the change magnitude (observed values minus predicted values) as an indicator [55]. We calculated the overall accuracy using visual interpretation sample points in the study area to determine an optimal threshold for change magnitude. Subsequently, we applied this threshold to classify the breaks identified by the CCDC algorithm, selecting

those with change magnitudes exceeding the threshold and considering the corresponding dates as indicative of forest disturbance occurrence. The optimal threshold selection for the two study regions is presented in Table 1. To further improve the accuracy of our results, we implemented two post-processing steps based on spatial information. Isolated pixels that were erroneously classified as disturbed were removed from the final degradation map. This step aimed to enhance the overall accuracy by mitigating misclassifications.

Table 1. Testing to find the optimal thresholds for monitoring forest loss.

Study Area	Sample Size	Step Size	Optimal Threshold	Overall Accuracy at Optimal Threshold
Study area I in Amazon	134	0.05	−0.25	93.68%
Study area II in Amazon	171	0.05	−0.26	80.12%

3.3.2. Accuracy Assessment of Forest Loss Detection Results

This study encompasses the selection of two local study areas within the Amazon research region. The precise distribution of these research areas, along with the spatial arrangement of validation sample points, are visually depicted in Figure 7. Table 2 provides a statistical summary of the types and quantities of validation samples in the two local study areas. The methodology employed for the selection of these sample points has been comprehensively described in Section 2.4.2.
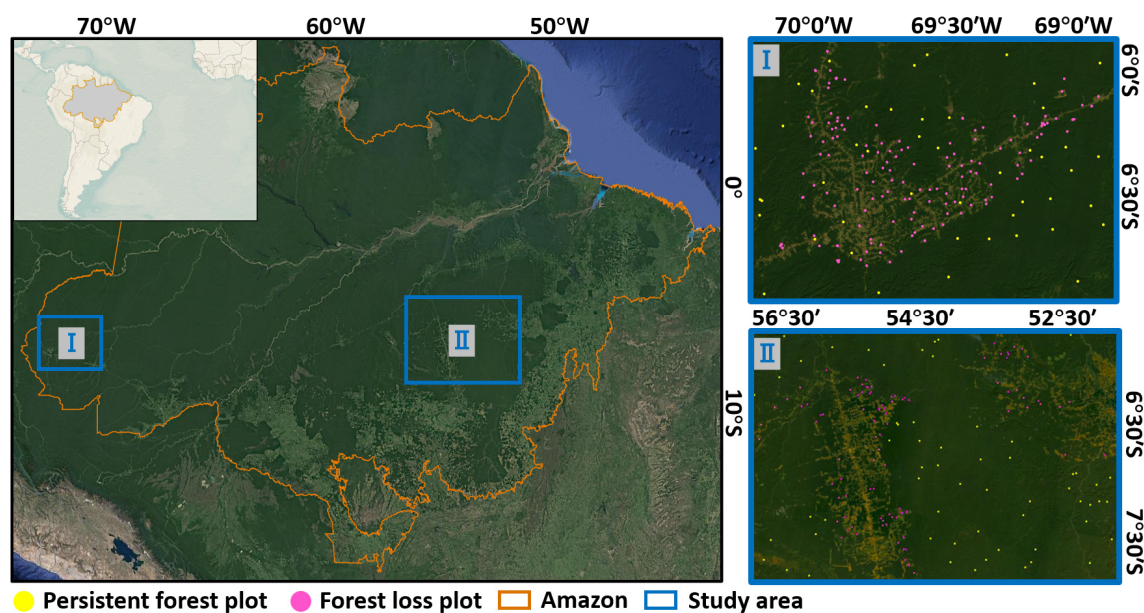
Figure 7. The local study area in the Amazon, as well as the number and distribution of sample points.

Table 2. Characteristics and quantities of the collected various sampling plot data.

		Forest Loss	Persistent Forest	Total
Study area I in Amazon	PRODES	43	37	80
	GEVI	51	23	74
Study area II in Amazon	PRODES	94	31	125
	GEVI	58	19	77
Total		246	110	356

The confusion matrices of the validation samples for the two local study areas are presented in Table 3. Comprehensive metrics and their corresponding interpretations can be found in Section 2.4.2. Specifically, in the validation conducted using sample points,

the producer and user accuracies for forest loss detections in the Amazon region's Study Area I and Study Area II exceeded 89%, respectively. The overall accuracy for these two areas was 86.00% and 88.31%, accompanied by Kappa coefficients of 0.78 and 0.76. Notably, the accuracy of the persistent type was notably lower than that of the loss type. This discrepancy can be attributed to the presence of loss-type pixels in close proximity to the sample points labeled as persistent type, resulting in misclassification within the 250-m pixel range. In conclusion, the combination of long-term GLASS FFC data and the CCDC algorithm proved effective for rapid and large-scale forest loss detection in both the Amazon region. The forest loss results obtained from this study provide a basis for further fine-grained classification using higher-resolution data, thus significantly saving time and resources.

Table 3. Accuracy assessment confusion matrix for forest loss in four study areas.

		Forest Loss	Persistent Forest	Producer's Accuracy	User's Accuracy	Overall Accuracy	Kappa
Study area I in Amazon	Forest loss in correct year	137	13	91.33%	90.13%	86.00%	0.78
	Persistent forest	15	35	70.00%	72.92%		
Study area II in Amazon	Forest loss in correct year	84	8	91.30%	89.36%	88.31%	0.76
	Persistent forest	10	52	83.87%	86.67%		

To enhance the clarity of the validation results, we conducted a spatial comparative analysis between the forest loss data provided by Global Forest Watch (GFW) from the Hansen Global Forest Change (GFC) database and the detection results from this study within the selected subregions (refer to Figure 8). Distinct colors are employed to depict loss areas corresponding to different years, with yellow indicating forest loss occurrences in 2000 and dark red representing those in 2020. The legend illustrates a gradual darkening pattern as the years progress. Simultaneously, we conducted an assessment of the temporal changes in forest loss areas across the study area. From 2000 to 2020, both the Amazon Forests exhibited a certain extent of forest loss due to a variety of frequent disturbance events. In the Amazon region, forest loss areas were primarily concentrated around areas characterized by intensive human activities, primarily resulting from timber harvesting and the conversion of forested land to bare land. Notably, the majority of detected forest loss areas were attributed to logging activities, as evidenced by the regularity observed in their boundary shapes. Analysis of the statistics concerning forest loss area changes in the study area revealed significant inter-annual variations from 2000 to 2020, owing to dynamic changes in forest management practices and disturbance patterns. In summary, the identification results obtained from this study generally align with the trends observed in the Hansen GFC data. However, the detected forest loss areas appear slightly larger due to the coarser spatial resolution used in this analysis.

Owing to the temporal richness exhibited in the data time series, the forest loss identification outcomes, utilizing GLASS FFC data and the CCDC algorithm, can achieve month-level precision. In this study, a representative region was selected to undertake spatial comparisons between Landsat imagery and forest loss detection results obtained for specific months. Figure 9 illustrates a close correspondence between the monthly progression of forest loss and the observed variations in Landsat images. Concurrently, the presence of cloud interference in Landsat images is evident, which poses challenges for monthly forest loss identification using this data source. Nevertheless, this underscores the advantages of our research methodology, despite the spatial resolution of our data being 250 m.
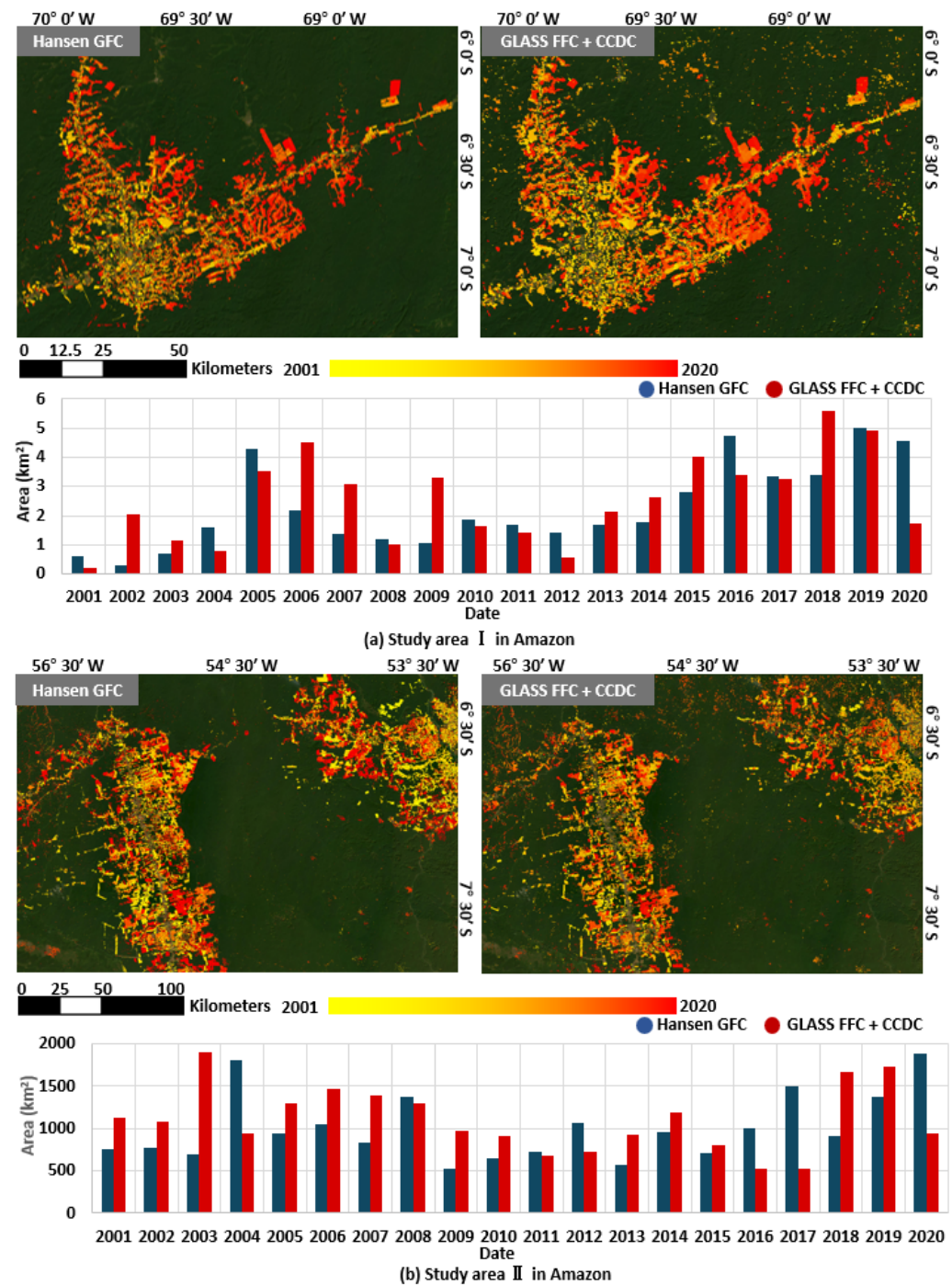
Figure 8. The annual forest loss identification results are based on GLASS FFC and CCDC algorithm in the Amazon study area, as well as the comparison with the validation data Hansen GFC. (**a**) Study area I is in Amazon; (**b**) Study area II is in Amazon.
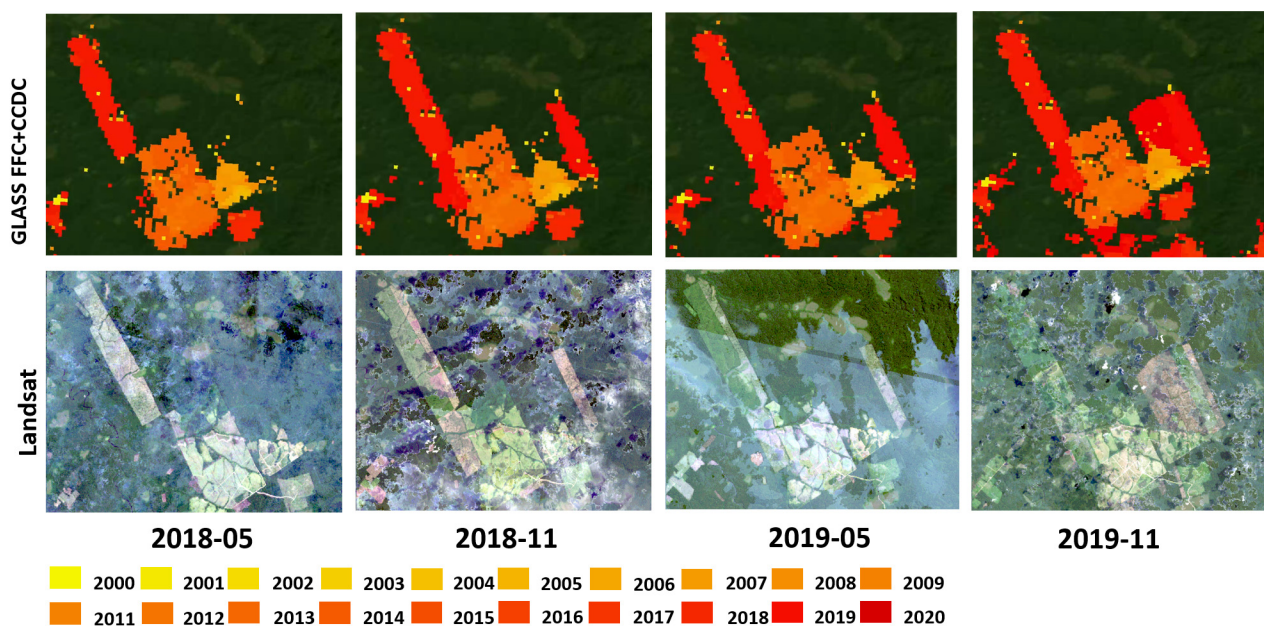
Figure 9. Spatial comparison of Landsat images and forest loss detection results across different months.

3.3.3. Comparison with Other Vegetation Datasets

As observed in the previous section, the developed methodology in this study presents a notable advantage in forest loss detection by effectively leveraging the abundant information contained within the time series of GLASS FFC data through the implementation of the CCDC algorithm. In this section, we will compare and analyze the proposed forest loss detection method with existing and commonly used combinations of vegetation index data and algorithms. In this section, we utilized a combination of MODIS VCF [10] and MODTrendr algorithms [60], with MODTrendr being an algorithm specifically tailored for MODIS data and an improvement over LandTrendr [61]. Additionally, we employed a combination of MODIS EVI [62] data and the CCDC algorithm. These data algorithm combinations were used to identify forest loss locations occurring within Study Area II (Figure 6) in the Amazon region from 2000 to 2020. The identified locations were compared with the Hansen GFC data in Figure 8b, and the results obtained through our proposed methodology, as shown in Figure 10. The validation sample points used for Study Area II were also retained and included in this section (Figure 6). The detailed statistical results are presented in Table 4.

Table 4. Accuracy assessment confusion matrix for forest loss in four study areas from different combinations of data and methods in Study area II in Amazon.

		Loss in Correct Year	Persistent Forest	Producer's Accuracy	User's Accuracy	Overall Accuracy	Kappa
GLASS FFC CCDC	Forest loss in correct year	84	8	91.30%	89.36%	88.31%	0.76
	Persistent forest	10	52	83.87%	86.67%		
MODIS VCF MODTrendr	Forest loss in correct year	57	11	83.82%	56.98%	68.83%	0.39
	Persistent forest	37	49	60.64%	81.67%		
MODIS EVI CCDC	Forest loss in correct year	34	6	85.00%	36.17%	57.14%	0.25
	Persistent forest	60	54	51.92%	90.00%		
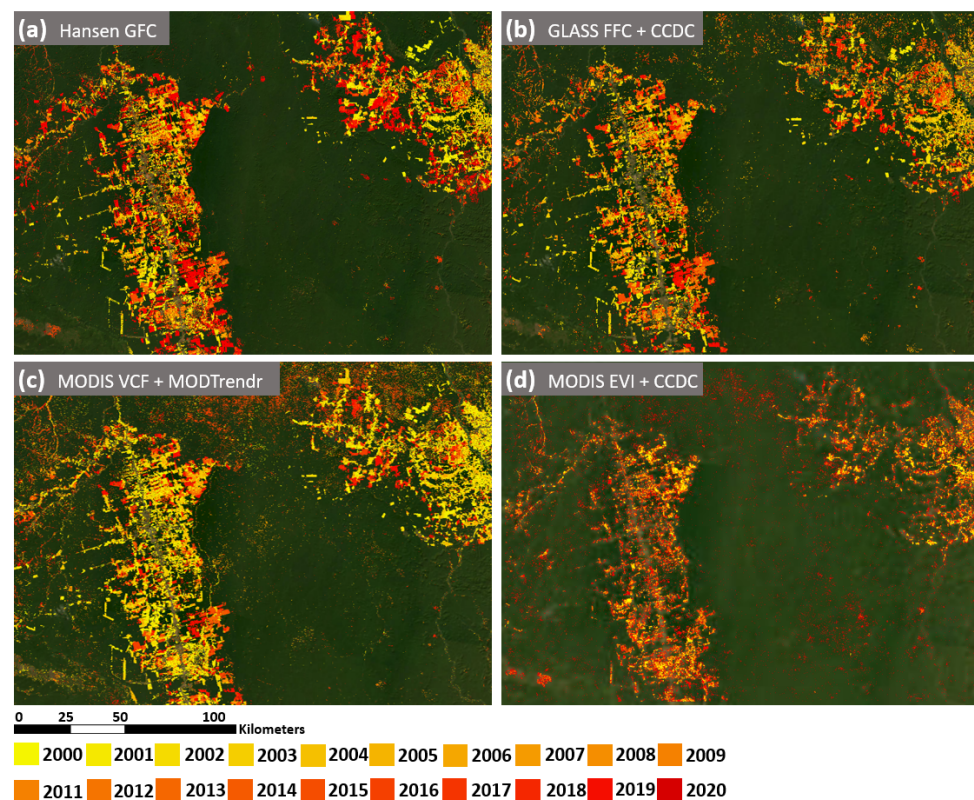
Figure 10. Consistency of year-to-year forest loss results from different combinations of data and methods. (**a**) The Hansen GFC. (**b**) Yearly Forest Loss Identification Results based on GLASS FFC and CCDC. (**c**) Yearly Forest Loss Identification Results based on MODIS VCF and MODTrendr. (**d**) Yearly Forest Loss Identification Results based on MODIS EVI and CCDC.

Yearly Forest Loss Identification Results based on MODIS EVI and CCDC.

Based on the findings presented in Figure 10 and Table 4, it was observed that the fusion of GLASS FFC data and the CCDC algorithm yielded the most accurate recognition outcomes, as evidenced by the highest validation accuracy of the sample points. Conversely, the combination of MODIS VCF and MODTrendr exhibited a distinct delineation of the recognized areas; however, its accuracy in detecting the specific year of forest loss deviated more from the actual results. The combination of MODIS EVI data and the CCDC algorithm, on the other hand, displayed issues with incomplete recognition. In summary, the forest loss detection method employed in this study demonstrates certain advantages in the context of 250 m resolution data, enabling rapid and large-scale identification of forest loss. Nevertheless, when compared to higher-resolution vegetation index series and LiDAR data, there remains potential for further improvement in the methodology.

4. Discussion

4.1. Characteristics of GLASS FFC Data

Previous validation efforts conducted on MODIS VCF [45] have indicated that the estimated values of MODIS VCF throughout the entire tropical region did not exceed 80%, which is clearly inconsistent with the actual conditions. Therefore, we employed the same validation data and methodology to examine the performance of GLASS FFC, specifically in the tropical region. The validation methodology was adopted from the MODIS VCF literature [10]. We reprojected the GEDI-derived canopy cover data onto the GLASS FFC grid, limiting the validation dataset to GLASS FFC pixels containing five or more high-quality GEDI data points to minimize potential sampling errors in the aggregation process [45]. Subsequently, we averaged the tree canopy cover samples falling

within each MODIS pixel. Specifically, we assessed the occurrence of canopy cover at the footprint level across the entire Amazon region, resulting in over 450,000 sample points.

Figure 11 presents an illustration of the spatial distribution of GLASS FFC and GEDI footprints within the study area of the Amazon rainforest. In the Amazon region, a significant level of agreement was observed between the estimated canopy cover values derived from GEDI and GLASS FFC (R^2 = 0.7492, RMSE = 14.03%). Both datasets exhibited a bimodal distribution pattern in terms of canopy cover. However, the peaks of GLASS FFC were centered at 18% and 75%, whereas those of GEDI were centered at 8% and 85%. Notably, GLASS FFC displayed an additional minor peak at 8%. Furthermore, a high degree of consistency between the two datasets was found within the range of 25% to 65%, as evidenced by the overlapping cumulative probability curves. Previous studies have indicated that GEDI tends to exhibit higher mean values at the upper end of the range and lower values at the lower end [10]. The systematic discrepancy in higher values can be attributed to GEDI's inability to distinguish between trees and buildings, leading to an overestimation of canopy cover due to the misinterpretation of taller buildings as higher vegetation cover. This disparity contributes to the observed differences in the bimodal patterns between the two datasets. Simultaneously, in contrast to the phenomenon observed in MODIS VCF, where the values did not exceed 80% throughout the entire tropical region, as depicted in Figure 11c, GLASS FFC effectively mitigated this limitation.
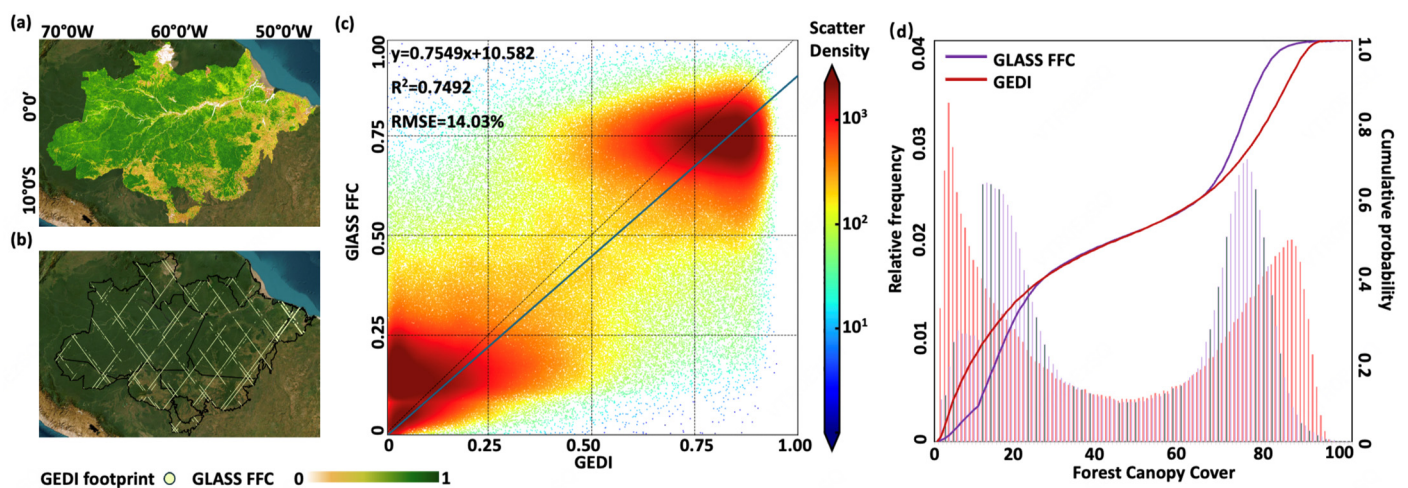
Figure 11. Comparison of GLASS FFC percent tree cover with GFCC percent canopy cover in the Amazon region. Panel (**a**) illustrates the spatial distribution of GLASS FFC in the Amazon region. Panel (**b**) presents the geographic extent of the GEDI flight lines in Amazon. Panel (**c**) shows a detailed comparison between GLASS FFC and GEDI sample points in the Amazon region. The blue line in the scatter plot is the linear regression line that fits the paired data points. In Panel (**d**), the thin bar lines represent the probability distribution of GEDI canopy cover (red) and GLASS FFC (purple) in the Amazon region, while the solid line corresponds to their respective cumulative distribution functions.

4.2. Application Potential and Prospects

The GLASS FFC dataset represents the first set of 8-day resolution forest cover data. In comparison to other long-term, high-temporal-resolution vegetation indices, it provides a more effective and intuitive means of monitoring forest dynamics. This efficacy stems from the fact that forest loss or recovery is defined by the decrease or increase in forest cover [63,64]. Regarding the application of GLASS FFC, one aspect involves the utilization of dense intra-annual and inter-annual trend information to ascertain the precise months and seasons during which forest loss transpires within distinct climatic zones. Alternatively, gaining a more nuanced understanding of the underlying drivers of forest disturbances [65] (including natural degradation, anthropogenic logging, wildfires, and

insect infestations) relies on the analysis of temporal characteristics and patterns [66]. Additionally, the temporal regularities within the GLASS FFC data also enable the assessment of subsequent recovery or afforestation efforts. By monitoring changes in forest cover over time, researchers can evaluate the effectiveness and success of restoration initiatives or reforestation programs. This critical evaluation contributes to a comprehensive comprehension of the causes of global forest disturbances and their environmental consequences on a global scale. Moreover, it provides valuable insights for sustainable forest management and conservation strategies.

Subsequent research endeavors concerning the GLASS FFC data will primarily concentrate on leveraging its dense time-series information to achieve a more precise mapping of forest disturbances on a global scale. Firstly, efforts are directed towards integrating the attention mechanism with deep learning methodologies to extract the most pertinent historical forest cover information. The attention mechanism can be employed to prioritize and extract the most significant features from the dense time-series data [67,68]. When applied to the GLASS FFC data, the attention mechanism can be utilized to identify and emphasize the relevant historical forest cover information. This includes data from adjacent times within the same year, as well as data from the same time in different years. By assigning attention weights to different temporal instances, the model can effectively highlight the time points that provide important insights into forest disturbances. During the training process, the attention mechanism learns to assign higher weights to the most informative temporal instances while suppressing the influence of less relevant ones.

4.3. Limitations and Future Work

The methodology proposed in this study introduces the GLASS FFC data as an innovative approach for monitoring forest change and assessing disturbances, capitalizing on its advantageous attributes of high temporal resolution and extensive spatial coverage. However, it is crucial to acknowledge that the algorithms employed in this study primarily rely on GLASS FVC and MODIS VCF data, which raises the possibility of error amplification originating from the quality of the source data [25]. To address this concern, future research endeavors can employ existing forest cover data as a reference training set [69] and supplement it with a substantial volume of ground truth data or high-resolution satellite images for annotation and validation [70]. Furthermore, adopting more suitable algorithms, such as deep learning methods, can be pursued to advance the development of forest cover data with enhanced spatial and temporal resolutions [71–73]. It is noteworthy that forest cover exhibits high levels of diversity, encompassing various vegetation types, topographical features, and ecological conditions. Consequently, ensuring the robustness and generalization capability of deep learning models across diverse forest ecosystems poses a significant challenge that warrants careful consideration and further investigation.

5. Conclusions

This study introduces a novel methodology for constructing fractional forest cover data with a temporal resolution of eight days at a 250-m spatial resolution, based on the long-term series GLASS FVC product and the annual MODIS VCF product. Subsequently, the high-quality, long-term series forest cover data product, GLASS FFC, was developed to encompass global scales. This dataset represents the first suite capable of monitoring intra-annual and inter-annual dynamics of forest cover globally. For verification, the dataset was assessed both globally and at localized scales using the high spatial resolution data from the GFCC. Moreover, to explore the dataset's applicability in monitoring forest disturbances, an enhanced Continuous Change Detection and Classification (CCDC) algorithm was employed, enabling the rapid, large-scale detection of annual forest loss from 2000 to 2020 in two study areas within the Amazon. The specific research findings are as follows:

(1) By employing pixel-based time series plotting of FFC and its comparison with GLASS FVC, GLASS FFC has demonstrated the capability to accurately reflect seasonal variations and abrupt changes in forest cover within the year. The discrepancies and

convergences between GLASS FFC and vegetation cover provide new perspectives for identifying different land cover classifications and for detecting forest loss and recovery.

(2) The spatial validation of GLASS FFC with high-resolution GFCC data illustrates that this product achieves high accuracy across various continents and forest coverage scenarios globally. Validation results based on global sites show a coefficient of determination (R^2) of 0.9085 and an RMSE of 7.22%. Notably, the accuracy in the Eurasian continent is even higher, reaching an R^2 of 0.9352 and an RMSE of 6.58%. Furthermore, validation in the Amazon region using radar data demonstrates that GLASS FFC mitigates the limitation observed in MODIS VCF, where forest cover estimates in low-latitude tropical rainforest areas did not exceed 80%.

(3) Furthermore, the integration of GLASS FFC with the CCDC algorithm has achieved a detection accuracy exceeding 86% for forest loss in the Amazon rainforest region. At a 250-m spatial resolution, this approach effectively captured disturbances of various scales. To a certain extent, GLASS FFC surpasses vegetation indices such as NDVI, EVI, and NBR, establishing itself as a crucial indicator for describing the ecological status of forests.

Author Contributions: Conceptualization, W.S. and X.Z.; Data curation, W.S., L.S. and Q.W.; Formal analysis, W.S., S.Z. and Y.G.; Methodology, W.S. and X.Z.; Writing—review and editing, W.S., H.Y., S.Z. and Y.G. All authors have read and agreed to the published version of the manuscript.

Data Availability Statement: The raw data supporting the conclusions of this article will be made available by the authors upon request.

Conflicts of Interest: No potential conflict of interest was reported by the authors.

References

1. Palmer, L. How Trees and Forests Reduce Risks from Climate Change. *Nat. Clim. Chang.* **2021**, *11*, 374–377. [CrossRef]
2. Anderegg, W.R.L.; Trugman, A.T.; Badgley, G.; Anderson, C.M.; Bartuska, A.; Ciais, P.; Cullenward, D.; Field, C.B.; Freeman, J.; Goetz, S.J.; et al. Climate-Driven Risks to the Climate Mitigation Potential of Forests. *Science* **2020**, *368*, eaaz7005. [CrossRef] [PubMed]
3. Cook-Patton, S.C.; Leavitt, S.M.; Gibbs, D.; Harris, N.L.; Lister, K.; Anderson-Teixeira, K.J.; Briggs, R.D.; Chazdon, R.L.; Crowther, T.W.; Ellis, P.W.; et al. Mapping Carbon Accumulation Potential from Global Natural Forest Regrowth. *Nature* **2020**, *585*, 545–550. [CrossRef] [PubMed]
4. Sommerfeld, A.; Senf, C.; Buma, B.; D'Amato, A.W.; Després, T.; Díaz-Hormazábal, I.; Fraver, S.; Frelich, L.E.; Gutiérrez, Á.G.; Hart, S.J.; et al. Patterns and Drivers of Recent Disturbances across the Temperate Forest Biome. *Nat. Commun.* **2018**, *9*, 4355. [CrossRef] [PubMed]
5. Li, Y.; Wu, Z.; Xu, X.; Fan, H.; Tong, X.; Liu, J. Forest Disturbances and the Attribution Derived from Yearly Landsat Time Series over 1990–2020 in the Hengduan Mountains Region of Southwest China. *For. Ecosyst.* **2021**, *8*, 73. [CrossRef]
6. Hansen, M.C.; DeFries, R.S.; Townshend, J.R.G.; Carroll, M.; Dimiceli, C.; Sohlberg, R.A. Global Percent Tree Cover at a Spatial Resolution of 500 Meters: First Results of the MODIS Vegetation Continuous Fields Algorithm. *Earth Interact.* **2003**, *7*, 1–15. [CrossRef]
7. Jia, K.; Liang, S.; Wei, X.; Li, Q.; Du, X.; Jiang, B.; Yao, Y.; Zhao, X.; Li, Y. Fractional Forest Cover Changes in Northeast China from 1982 to 2011 and Its Relationship with Climatic Variations. *IEEE J. Sel. Top. Appl. Earth Obs. Remote Sens.* **2015**, *8*, 775–783. [CrossRef]
8. Liu, X.; Liang, S.; Li, B.; Ma, H.; He, T. Mapping 30 m Fractional Forest Cover over China's Three-North Region from Landsat-8 Data Using Ensemble Machine Learning Methods. *Remote Sens.* **2021**, *13*, 2592. [CrossRef]
9. Pradhan, P.; Costa, L.; Rybski, D.; Lucht, W.; Kropp, J.P. A Systematic Study of Sustainable Development Goal (SDG) Interactions. *Earth's Future* **2017**, *5*, 1169–1179. [CrossRef]

10. DiMiceli, C.; Townshend, J.; Carroll, M.; Sohlberg, R. Evolution of the Representation of Global Vegetation by Vegetation Continuous Fields. *Remote Sens. Environ.* **2021**, *254*, 112271. [CrossRef]

11. Hansen, M.; DiMiceli, C.; Sohlberg, R. *User Guide for the MEaSURES Vegetation Continuous Fields Product, Version 1*; University of Maryland: College Park, MD, USA, 2017.

12. Sexton, J.O.; Song, X.-P.; Feng, M.; Noojipady, P.; Anand, A.; Huang, C.; Kim, D.-H.; Collins, K.M.; Channan, S.; DiMiceli, C.; et al. Global, 30-m Resolution Continuous Fields of Tree Cover: Landsat-Based Rescaling of MODIS Vegetation Continuous Fields with Lidar-Based Estimates of Error. *Int. J. Digit. Earth* **2013**, *6*, 427–448. [CrossRef]

13. Shimada, M.; Isoguchi, O.; Motooka, T.; Shiraishi, T.; Mukaida, A.; Okumura, H.; Otaki, T.; Itoh, T. Generation of 10 m Resolution PALSAR and JERS-SAR Mosaic and Forest/Non-Forest Maps for Forest Carbon Tracking. In Proceedings of the 2011 IEEE International Geoscience and Remote Sensing Symposium, Vancouver, BC, Canada, 24–29 July 2011; Available online: https://ieeexplore.ieee.org/abstract/document/6049978 (accessed on 21 April 2024).

14. Hansen, M.C.; Potapov, P.V.; Moore, R.; Hancher, M.; Turubanova, S.A.; Tyukavina, A.; Thau, D.; Stehman, S.V.; Goetz, S.J.; Loveland, T.R.; et al. High-Resolution Global Maps of 21st-Century Forest Cover Change. *Science* **2013**, *342*, 850–853. [CrossRef] [PubMed]

15. Hansen, M.C.; Egorov, A.; Roy, D.P.; Potapov, P.; Ju, J.; Turubanova, S.; Kommareddy, I.; Loveland, T.R. Continuous Fields of Land Cover for the Conterminous United States Using Landsat Data: First Results from the Web-Enabled Landsat Data (WELD) Project. *Remote Sens. Lett.* **2011**, *2*, 279–288. [CrossRef]

16. Liu, X.; Liang, S.; Ma, H.; Li, B.; Zhang, Y.; Li, Y.; He, T.; Zhang, G.; Xu, J.; Xiong, C.; et al. Landsat-Observed Changes in Forest Cover and Attribution Analysis over Northern China from 1996–2020. *GIScience Remote Sens.* **2024**, *61*, 2300214. [CrossRef]

17. Yan, Y.; Piao, S.; Hammond, W.M.; Chen, A.; Hong, S.; Xu, H.; Munson, S.M.; Myneni, R.B.; Allen, C.D. Climate-Induced Tree-Mortality Pulses Are Obscured by Broad-Scale and Long-Term Greening. *Nat. Ecol. Evol.* **2024**, *8*, 912–923. [CrossRef]

18. Shimizu, K.; Ota, T.; Mizoue, N. Accuracy Assessments of Local and Global Forest Change Data to Estimate Annual Disturbances in Temperate Forests. *Remote Sens.* **2020**, *12*, 2438. [CrossRef]

19. Galiatsatos, N.; Donoghue, D.N.; Watt, P.; Bholanath, P.; Pickering, J.; Hansen, M.C.; Mahmood, A.R. An Assessment of Global Forest Change Datasets for National Forest Monitoring and Reporting. *Remote Sens.* **2020**, *12*, 1790. [CrossRef]

20. Frantz, D.; Röder, A.; Udelhoven, T.; Schmidt, M. Forest Disturbance Mapping Using Dense Synthetic Landsat/MODIS Time-Series and Permutation-Based Disturbance Index Detection. *Remote Sens.* **2016**, *8*, 277. [CrossRef]

21. Tang, X.; Bullock, E.L.; Olofsson, P.; Woodcock, C.E. Can VIIRS Continue the Legacy of MODIS for near Real-Time Monitoring of Tropical Forest Disturbance? *Remote Sens. Environ.* **2020**, *249*, 112024. [CrossRef]

22. Tang, X.; Bullock, E.L.; Olofsson, P.; Estel, S.; Woodcock, C.E. Near Real-Time Monitoring of Tropical Forest Disturbance: New Algorithms and Assessment Framework. *Remote Sens. Environ.* **2019**, *224*, 202–218. [CrossRef]

23. Ferrara, C.; Marchi, M.; Fabbio, G.; Fares, S.; Bertini, G.; Piovosi, M.; Salvati, L. Exploring Nonlinear Intra-Annual Growth Dynamics in *Fagus sylvatica* L. Trees at the Italian ICP-Forests Level II Network. *Forests* **2019**, *10*, 584. [CrossRef]

24. Martínez-Sancho, E.; Gutiérrez, E.; Valeriano, C.; Ribas, M.; Popkova, M.I.; Shishov, V.V.; Dorado-Liñán, I. Intra- and Inter-Annual Growth Patterns of a Mixed Pine-Oak Forest under Mediterranean Climate. *Forests* **2021**, *12*, 1746. [CrossRef]

25. Stanimirova, R.; Tarrio, K.; Turlej, K.; McAvoy, K.; Stonebrook, S.; Hu, K.-T.; Arévalo, P.; Bullock, E.L.; Zhang, Y.; Woodcock, C.E.; et al. A Global Land Cover Training Dataset from 1984 to 2020. *Sci. Data* **2023**, *10*, 879. [CrossRef] [PubMed]

26. Halperin, J.; LeMay, V.; Coops, N.; Verchot, L.; Marshall, P.; Lochhead, K. Canopy cover estimation in miombo woodlands of Zambia: Comparison of Landsat 8 OLI versus RapidEye imagery using parametric, nonparametric, and semiparametric methods. *Remote. Sens. Environ.* **2016**, *179*, 170–182. [CrossRef]

27. Jia, T.; Li, Y.; Shi, W.; Zhu, L. Deriving a Forest Cover Map in Kyrgyzstan Using a Hybrid Fusion Strategy. *Remote. Sens.* **2019**, *11*, 2325. [CrossRef]

28. De Jong, R.; de Bruin, S.; de Wit, A.; Schaepman, M.E.; Dent, D.L. Analysis of Monotonic Greening and Browning Trends from Global NDVI Time-Series. *Remote Sens. Environ.* **2011**, *115*, 692–702. [CrossRef]

29. Kokubu, Y.; Hara, S.; Tani, A. Mapping Seasonal Tree Canopy Cover and Leaf Area Using Worldview-2/3 Satellite Imagery: A Megacity-Scale Case Study in Tokyo Urban Area. *Remote Sens.* **2020**, *12*, 1505. [CrossRef]

30. Tucker, C.J. Red and Photographic Infrared Linear Combinations for Monitoring Vegetation. *Remote Sens. Environ.* **1979**, *8*, 127–150. [CrossRef]

31. Liu, L.; Zhang, X.; Gao, Y.; Chen, X.; Shuai, X.; Mi, J. Finer-Resolution Mapping of Global Land Cover: Recent Developments, Consistency Analysis, and Prospects. *J. Remote Sens.* **2021**, *2021*, 5289697. [CrossRef]

32. Yang, L.; Jia, K.; Liang, S.; Liu, J.; Wang, X. Comparison of Four Machine Learning Methods for Generating the GLASS Fractional Vegetation Cover Product from MODIS Data. *Remote Sens.* **2016**, *8*, 682. [CrossRef]

33. Jia, K.; Liang, S.; Liu, S.; Li, Y.; Xiao, Z.; Yao, Y.; Jiang, B.; Zhao, X.; Wang, X.; Xu, S.; et al. Global Land Surface Fractional Vegetation Cover Estimation Using General Regression Neural Networks from MODIS Surface Reflectance. *IEEE Trans. Geosci. Remote Sens.* **2015**, *53*, 4787–4796. [CrossRef]

34. North, P.R. Estimation of fAPAR, LAI, and Vegetation Fractional Cover from ATSR-2 Imagery. *Remote Sens. Environ.* **2002**, *80*, 114–121. [CrossRef]

35. Jia, K.; Yang, L.; Liang, S.; Xiao, Z.; Zhao, X.; Yao, Y.; Zhang, X.; Jiang, B.; Liu, D. Long-Term Global Land Surface Satellite (GLASS) Fractional Vegetation Cover Product Derived from MODIS and AVHRR Data. *IEEE J. Sel. Top. Appl. Earth Obs. Remote Sens.* **2018**, *12*, 508–518. [CrossRef]

36. Jia, K.; Liang, S.; Wei, X.; Yao, Y.; Yang, L.; Zhang, X.; Liu, D. Validation of Global LAnd Surface Satellite (GLASS) Fractional Vegetation Cover Product from MODIS Data in an Agricultural Region. *Remote Sens. Lett.* **2018**, *9*, 847–856. [CrossRef]

37. Xiong, C.; Ma, H.; Liang, S.; He, T.; Zhang, Y.; Zhang, G.; Xu, J. Improved Global 250 m 8-Day NDVI and EVI Products from 2000–2021 Using the LSTM Model. *Sci. Data* **2023**, *10*, 800. [CrossRef]

38. Song, X.-P.; Huang, C.; Sexton, J.O.; Channan, S.; Townshend, J.R. Annual Detection of Forest Cover Loss Using Time Series Satellite Measurements of Percent Tree Cover. *Remote Sens.* **2014**, *6*, 8878–8903. [CrossRef]

39. Tang, H.; Armston, J.; Dubayah, R. *Algorithm Theoretical Basis Document (ATBD) for GEDI L2B Footprint Canopy Cover and Vertical Profile Metrics*; Goddard Space Flight Center: Greenbelt, MD, USA, 2019.

40. Hoffrén, R.; Lamelas, M.T.; de la Riva, J.; Domingo, D.; Montealegre, A.L.; García-Martín, A.; Revilla, S. Assessing GEDI-NASA System for Forest Fuels Classification Using Machine Learning Techniques. *Int. J. Appl. Earth Obs. Geoinf.* **2023**, *116*, 103175. [CrossRef]

41. Tang, H.; Song, X.-P.; Zhao, F.A.; Strahler, A.H.; Schaaf, C.L.; Goetz, S.; Huang, C.; Hansen, M.C.; Dubayah, R. Definition and Measurement of Tree Cover: A Comparative Analysis of Field-, Lidar-and Landsat-Based Tree Cover Estimations in the Sierra National Forests, USA. *Agric. For. Meteorol.* **2019**, *268*, 258–268. [CrossRef]

42. Fayad, I.; Baghdadi, N.; Lahssini, K. An Assessment of the GEDI Lasers' Capabilities in Detecting Canopy Tops and Their Penetration in a Densely Vegetated, Tropical Area. *Remote Sens.* **2022**, *14*, 2969. [CrossRef]

43. Adam, M.; Urbazaev, M.; Dubois, C.; Schmullius, C. Accuracy Assessment of GEDI Terrain Elevation and Canopy Height Estimates in European Temperate Forests: Influence of Environmental and Acquisition Parameters. *Remote Sens.* **2020**, *12*, 3948. [CrossRef]

44. Marselis, S.M.; Keil, P.; Chase, J.M.; Dubayah, R. The Use of GEDI Canopy Structure for Explaining Variation in Tree Species Richness in Natural Forests. *Environ. Res. Lett.* **2022**, *17*, 045003. [CrossRef]

45. Tang, H.; Armston, J.; Hancock, S.; Marselis, S.; Goetz, S.; Dubayah, R. Characterizing Global Forest Canopy Cover Distribution Using Spaceborne Lidar. *Remote Sens. Environ.* **2019**, *231*, 111262. [CrossRef]

46. Chen, J.; Chen, J.; Liao, A.; Cao, X.; Chen, L.; Chen, X.; He, C.; Han, G.; Peng, S.; Lu, M.; et al. Global Land Cover Mapping at 30 m Resolution: A POK-Based Operational Approach. *ISPRS J. Photogramm. Remote Sens.* **2015**, *103*, 7–27. [CrossRef]

47. McDowell, N.G.; Allen, C.D.; Anderson-Teixeira, K.; Aukema, B.H.; Bond-Lamberty, B.; Chini, L.; Clark, J.S.; Dietze, M.; Grossiord, C.; Hanbury-Brown, A.; et al. Pervasive Shifts in Forest Dynamics in a Changing World. *Science* **2020**, *368*, eaaz9463. [CrossRef] [PubMed]

48. Bastin, J.-F.; Finegold, Y.; Garcia, C.; Mollicone, D.; Rezende, M.; Routh, D.; Zohner, C.M.; Crowther, T.W. The Global Tree Restoration Potential. *Science* **2019**, *365*, 76–79. [CrossRef] [PubMed]

49. Feng, Y.; Ziegler, A.D.; Elsen, P.R.; Liu, Y.; He, X.; Spracklen, D.V.; Holden, J.; Jiang, X.; Zheng, C.; Zeng, Z. Upward Expansion and Acceleration of Forest Clearance in the Mountains of Southeast Asia. *Nat. Sustain.* **2021**, *4*, 892–899. [CrossRef]

50. Wang, H.; Cai, L.; Wen, X.; Fan, D.; Wang, Y. Land Cover Change and Multiple Remotely Sensed Datasets Consistency in China. *Ecosyst. Health Sustain.* **2022**, *8*, 2040385. [CrossRef]

51. Andreacci, F.; Marenzi, R.C. Accounting for Twenty-First-Century Annual Forest Loss in the Atlantic Forest of Brazil Using High-Resolution Global Maps. *Int. J. Remote Sens.* **2020**, *41*, 4408–4420. [CrossRef]

52. Cunningham, D.; Cunningham, P.; Fagan, M.E. Identifying Biases in Global Tree Cover Products: A Case Study in Costa Rica. *Forests* **2019**, *10*, 853. [CrossRef]

53. Zhu, Z.; Woodcock, C.E. Continuous Change Detection and Classification of Land Cover Using All Available Landsat Data. *Remote Sens. Environ.* **2014**, *144*, 152–171. [CrossRef]

54. Pasquarella, V.J.; Arévalo, P.; Bratley, K.H.; Bullock, E.L.; Gorelick, N.; Yang, Z.; Kennedy, R.E. Demystifying LandTrendr and CCDC Temporal Segmentation. *Int. J. Appl. Earth Obs. Geoinf.* **2022**, *110*, 102806. [CrossRef]

55. Chen, S.; Woodcock, C.E.; Bullock, E.L.; Arévalo, P.; Torchinava, P.; Peng, S.; Olofsson, P. Monitoring Temperate Forest Degradation on Google Earth Engine Using Landsat Time Series Analysis. *Remote Sens. Environ.* **2021**, *265*, 112648. [CrossRef]

56. Shimizu, K.; Ota, T.; Mizoue, N.; Yoshida, S. A Comprehensive Evaluation of Disturbance Agent Classification Approaches: Strengths of Ensemble Classification, Multiple Indices, Spatio-Temporal Variables, and Direct Prediction. *ISPRS J. Photogramm. Remote Sens.* **2019**, *158*, 99–112. [CrossRef]

57. Arévalo, P.; Bullock, E.L.; Woodcock, C.E.; Olofsson, P. A Suite of Tools for Continuous Land Change Monitoring in Google Earth Engine. *Front. Clim.* **2020**, *2*, 576740. [CrossRef]

58. Shimabukuro, Y.E.; Santos, J.; Formaggio, A.; Duarte, V.; Rudorff, B.; Achard, F.; Hansen, M. The Brazilian Amazon monitoring program: PRODES and DETER projects. *Glob. For. Monit. Earth Obs.* **2016**, *2012*, 153–169.

59. Garrigues, S.; Lacaze, R.; Baret, F.J.T.M.; Morisette, J.T.; Weiss, M.; Nickeson, J.E.; Fernandeset, R. Validation and intercomparison of global Leaf Area Index products derived from remote sensing data. *J. Geophys. Res. Biogeosci.* **2008**, *113*, G2. [CrossRef]

60. Sulla-Menashe, D.; Kennedy, R.E.; Yang, Z.; Braaten, J.; Krankina, O.N.; Friedl, M.A. Detecting Forest Disturbance in the Pacific Northwest from MODIS Time Series Using Temporal Segmentation. *Remote Sens. Environ.* **2014**, *151*, 114–123. [CrossRef]

61. Li, M.; Huang, C.; Zhu, Z.; Shi, H.; Lu, H.; Peng, S. Assessing Rates of Forest Change and Fragmentation in Alabama, USA, Using the Vegetation Change Tracker Model. *For. Ecol. Manag.* **2009**, *257*, 1480–1488. [CrossRef]
62. Rahman, A.F.; Sims, D.A.; Cordova, V.D.; El-Masri, B.Z. Potential of MODIS EVI and Surface Temperature for Directly Estimating Per-Pixel Ecosystem C Fluxes. *Geophys. Res. Lett.* **2005**, *32*, L19404. [CrossRef]
63. Marshall, A.R.; Waite, C.E.; Pfeifer, M.; Banin, L.F.; Rakotonarivo, S.; Chomba, S.; Herbohn, J.; Gilmour, D.A.; Brown, M.; Chazdon, R.L. Fifteen Essential Science Advances Needed for Effective Restoration of the World's Forest Landscapes. *Philos. Trans. R. Soc. Lond. B Biol. Sci.* **2022**, *378*, 20210065. [CrossRef]
64. Liu, Y.; Ziegler, A.D.; Wu, J.; Liang, S.; Wang, D.; Xu, R.; Duangnamon, D.; Li, H.; Zeng, Z. Effectiveness of Protected Areas in Preventing Forest Loss in a Tropical Mountain Region. *Ecol. Indic.* **2022**, *136*, 108697. [CrossRef]
65. Altman, J.; Fibich, P.; Trotsiuk, V.; Altmanova, N. Global Pattern of Forest Disturbances and Its Shift under Climate Change. *Sci. Total Environ.* **2024**, *915*, 170117. [CrossRef] [PubMed]
66. Pickering, J.; Stehman, S.V.; Tyukavina, A.; Potapov, P.; Watt, P.; Jantz, S.M.; Bholanath, P.; Hansen, M.C. Quantifying the Trade-off between Cost and Precision in Estimating Area of Forest Loss and Degradation Using Probability Sampling in Guyana. *Remote Sens. Environ.* **2019**, *221*, 122–135. [CrossRef]
67. Yuan, Y.; Lin, L. Self-Supervised Pretraining of Transformers for Satellite Image Time Series Classification. *IEEE J. Sel. Top. Appl. Earth Obs. Remote Sens.* **2021**, *14*, 474–487. [CrossRef]
68. Yuan, Y.; Lin, L.; Huo, L.-Z.; Kong, Y.-L.; Zhou, Z.-G.; Wu, B.; Jia, Y. Using An Attention-Based LSTM Encoder–Decoder Network for Near Real-Time Disturbance Detection. *IEEE J. Sel. Top. Appl. Earth Obs. Remote Sens.* **2020**, *13*, 1819–1832. [CrossRef]
69. Hasan, M.E.; Nath, B.; Sarker, A.H.M.R.; Wang, Z.; Zhang, L.; Yang, X.; Nobi, M.N.; Røskaft, E.; Chivers, D.J.; Suza, M. Applying Multi-Temporal Landsat Satellite Data and Markov-Cellular Automata to Predict Forest Cover Change and Forest Degradation of Sundarban Reserve Forest, Bangladesh. *Forests* **2020**, *11*, 1016. [CrossRef]
70. Vieilledent, G.; Grinand, C.; Rakotomalala, F.A.; Ranaivosoa, R.; Rakotoarijaona, J.-R.; Allnutt, T.F.; Achard, F. Combining Global Tree Cover Loss Data with Historical National Forest Cover Maps to Look at Six Decades of Deforestation and Forest Fragmentation in Madagascar. *Biol. Conserv.* **2018**, *222*, 189–197. [CrossRef]
71. Aziz, G.; Minallah, N.; Saeed, A.; Frnda, J.; Khan, W. Remote Sensing Based Forest Cover Classification Using Machine Learning. *Sci. Rep.* **2024**, *14*, 69. [CrossRef] [PubMed]
72. Tariq, A.; Jiango, Y.; Li, Q.; Gao, J.; Lu, L.; Soufan, W.; Almutairi, K.F.; Habib-ur-Rahman, M. Modelling, Mapping and Monitoring of Forest Cover Changes, Using Support Vector Machine, Kernel Logistic Regression and Naive Bayes Tree Models with Optical Remote Sensing Data. *Heliyon* **2023**, *9*, e13212. [CrossRef]
73. Kennedy, R.E.; Yang, Z.; Cohen, W.B.; Pfaff, E.; Braaten, J.; Nelson, P. Spatial and Temporal Patterns of Forest Disturbance and Regrowth within the Area of the Northwest Forest Plan. *Remote Sens. Environ.* **2012**, *122*, 117–133. [CrossRef]